# Dynamics of an Excess Electron in Water

by

Ickjin Park
M.Sc., Seoul National University
B.Sc., Seoul National University

Submitted to the Department of Physics
in partial fulfillment of the requirements for the degree of

Doctor of Philosophy

at the

MASSACHUSETTS INSTITUTE OF TECHNOLOGY

June 1999



Author .....
Department of Physics
April 12, 1999

Certified by .....
John D. Joannopoulos
Francis Wright Davis Professor of Physics
Thesis Supervisor

Accepted by .....
Thomas Greytak
Associate Department Head for Education

# Dynamics of an Excess Electron in Water

by

Ickjin Park

M.Sc., Seoul National University

B.Sc., Seoul National University

Submitted to the Department of Physics
on April 12, 1999, in partial fulfillment of the
requirements for the degree of
Doctor of Philosophy

## Abstract

In recent years, first principles investigations have been applied successfully to the calculation of the electronic and geometric structures of bulk solids. In this thesis, I have concentrated on extending this territory toward the realm of molecules and liquids. As a first step in this direction, I describe calculations of hydrogen adsorption on the classic (111)-(7×7) reconstructed surface of Si. The myriad of dangling bond sites on this extremely complex surface offer a unique "laboratory" in which to study atom-surface interactions. As a next step, I then apply the same theoretical foundation to study the molecular complex $(H_2O)_6^-$. Such clusters of water molecules can be created in fine-mists but, other than their existence, very little is known about them either experimentally or theoretically. By combining state-of-the-art quantum chemical and first-principles density functional techniques, this study not only results in a wide range of new predictions but also helps establish the validity of the first-principles approach to the case of non-solid environments. Finally, I introduce the concept of a *molecular* pseudopotential in order to investigate, in a tractable first-principles fashion, the physical and chemical properties of an excess electron migrating through bulk liquid water at room temperature. These calculations successfully reveal, for the very first time, the intricate and microscopic process associated with electron transport in this fundamental system.

Thesis Supervisor: John D. Joannopoulos
Title: Francis Wright Davis Professor of Physics

*TO MY FAMILY*

# Acknowledgments

First, I would like to express my sincere gratitude to my advisor Prof. John D. Joannopoulos for his generous guidance throughout my graduate studies. For six years at MIT, he has supported me with patience, care, and encouragement. It has been a great honor for me to have opportunities of having a glance into his deep understanding of physics in general. I have borrowed a great deal from his thoughtful insight in my study of the wet electron. I feel any flaw in this thesis is the result of my inaccurate peeping into his world, and I am fully responsible. I am also indebted to John for helping me grow as an individual. Whenever someone finds me more patient, more diligent and kinder than I once was, I give the credit to John. Moreover, his humane sense of decency will be well-kept in my heart with great appreciation.

I am also eager to reveal my artless appreciation to Kyeongjae Cho for most pleasant hours in collaboration. He has always been available for me and kind enough not to show any sign of tiresomeness. I have greatly benefited from his penetrating intuition in physics and have been continually stimulated by his critical thinking. In addition, he has been indispensable for me to maintain my good command of Korean.

I have been fortunate to work with many venerable visiting scholars. I am grateful to Prof. H. Lim, Prof. K.S. Kim, and Dr. Sik Lee for all the entertaining discussion, pleasant interaction, and productive collaboration. The days and nights I struggled with Sik Lee were some of the best times during my stay in Cambridge. My latest encounter with a visiting scholar, Nikolaj Moll, has brought me many more pleasurable moments. His generosity of sharing his magic spells in LaTeX should be praised as an act of a good Samaritan.

I am also grateful to Prof. Tomás Arias for all the congenial discussion about physics and computers. His door was always open and welcoming. I am one of the most benefitted by his beautiful codes. He has also kindly agreed to serve on my thesis committee with Prof. Earle L. Lomon. I thank them both for their careful reading and thoughtful comments on this thesis.

My officemates have been extremely kind to me: They never complained about

the garlic smell. In particular, Rodrigo Capaz and Tairan Wang have provided very amusing occasions. By interacting with them scientifically and socially, I have learned, in many ways, how to effectively communicate with others. I also wish to pay my supreme homage to other fellow sheep under *Shepherd John*: Shanhui Fan, Steven G. Johnson, Attila Mekis, Evan Reed, Maksim Skorobogatiy, and Pierre Villeneuve. I specially thank Evan for his careful proof-reading. Another special thank-you is due to CMT secretary Margaret E. O'meara. She has been simply wonderful.

In Cambridge, Hyunwoo Lee and I survived the dark bachelorhood together for more than three years as roommates. I am very grateful to him for keeping me healthy with his professional cooking. I am also grateful to other Korean friends: K.W. Ahn, K.S. Joo, H.S. Chung, W. Woo, H.C. Kim, D.S. Park, T. Shin, Y.G. Park, Y.B. Kim, S. Park, and D.H. Kim. Paticularly pleasant were gatherings with former CMT members, Y.B. Kim and D.H. Kim.

At one point in my life, H.S. Chung happily agreed to be my god-father, for which I am always thankful. In this same spirit, D.P. Min, J.K. Lee, S.J. Oh, and J.S. Ihm took the responsibility of being my mentors during my studies in Korea. I thank them all.

Finally, I am deeply indebted to my parents and parents-in-law. Only with their endless love and sacrifice could I be here. And last but not least, I would like to thank my wife, Miran, and my kids, Yejoo and Ian, for their love and patience. I seek their generous forgiveness for my negligence as a husband and father.

# Contents

# List of Figures

# List of Tables

# Chapter 1

# Introduction

Ever since the early days of quantum mechanics, physicists have been trying to understand material properties not only by experiments but also by direct solution of Schrödinger's equation. One such approach, which has proven very successful in recent years, involves calculation of the total energy of a solid from first principles. The basic idea is to calculate the ground state configuration of a many-body system of interacting electrons and nuclei given only the atomic numbers of the constituent elements as input. This of course is completely intractable without the imposition of several approximations. These approximations, however, turn out to be well founded and robust, so that physicists are currently, and perhaps routinely, performing accurate calculations to predict the electronic and geometric structures of defects, surfaces and interfaces in solids, the migration properties of impurities and self-interstitials in solids, the properties of structural phase transitions of solids, and even the electronic and geometric structures of novel materials. Most recently, some progress has even been made toward utilizing first principles techniques to study problems in the biomolecular arena.

The success of the first principles approach lies in the multitude of work that has been performed to fine-tune and improve its various approximations. The first basic approximation involves the so-called adiabatic or Born-Oppenheimer approximation. Since the electrons are much lighter than the nuclei, yet the forces between the particles are the same, the electrons essentially respond instantaneously to any

motion of the nuclei. This separation of variables in the many body wavefunction is a significant simplication to the original problem. Nevertheless, it is still not sufficient to enable tractable calculations of the ground state. This only becomes possible with the Density Functional Theory (DFT) by Hohenberg, Kohn and Sham. Density Functional Theory [1, 2] allows one to map the ground state properties of the many body electron system in any external single-particle potential to that of an equivalent system of "independent" electrons in the presence of an "effective" single-particle potential. Given the exact form for the energy density functional this mapping is exact! Although the energy desiity functional is not known precisely *a priori*, sufficiently good models have been introduced, such as the local density approximation (LDA) [2, 3, 4, 5, 6] and generalized gradient approximation (GGA) [7, 8, 9, 10], that this approach works very well in practice. It should be noted, however, that the "validity" and general acceptance of these model approximations has emerged only after many years of successful calculations of varying types of materials and systems.

Given the adiabatic and LDA/GGA approximations it is possible to perform total energy calculations of solids, but only for very small unit cells containing tens of atoms. The problem lies in the strong Coulomb interaction between the electrons and nuclei. Moreover, not all the electrons in a solid are important. In a typical atom, one can separate all the electrons into either core electrons or valence electrons. The core electrons are very tightly bound around the nucleus and for all practical purposes can be considered inert, both for the core of an isolated atom and an atom in a solid. Thus it is only the valence electrons that are important and that need to be considered. If one now considers that the valence electrons spend most of their time in the weaker parts of the potential outside the strong core potential region, one can envision replacing the true valence electrons with pseudo-electrons which are described by a weak core pseudopotential *everywhere* in space. This is the basis of the Pseudopotential Approximation [11, 12, 13]. In a practical sense, the reduction in the number of plane waves accompanied by the use of pseudopotentials is very important because it enables one to investigate systems composed of many more atoms.

But, even with all the fine work mentioned above, the conventional procedure

of directly diagonalizing matrices has been a cause of "poor" performance for many years. To make matters worse, direct diagonalization methods are memory inefficient because they require storage of all the individual entries of a matrix. In contrast, indirect diagonalization methods keep track of only low lying eigenstates, which results in an order of magnitude improvement in the speed and the memory usage. Without indirect diagonalization methods, it would not be possible to carry out first principles studies on systems composed of about 100 atoms, as is typical nowadays. Therefore the new iterative indirect diagonalization methods, as well as the ever-increasing computational power of super computers, must be also considered quite an essential ingredient in the present success of first principles calculations.

The synergistic outcome of all these theoretical and algorithmic advancements has been so great that one can now calculate the electronic structure of a system made up of 200 Si atoms in a week. So, it is not unusual to see results of first principles calculations begin to be used in other fields such as mechanical and chemical engineering to address *real* materials problems [14]. However, to meet the emerging interest in bio-chemical problems such as proton/electron transfer, protein folding, and enzymatic catalysis, the current methods in first principles calculations are not suitable. Most of the difficulties in applying first principles methods in bio-chemical systems originate from the simple fact that these systems are far larger than typical systems where first principles methods have been applied so far. As an example, Hemoglobin, one of the small bio-functional molecules, has 128 amino-acids. Since one amino-acid is made up of about 20 atoms on average, it means that one has to handle more than 2000 atoms. Even if we ignore that the strong pseudopotentials of carbon and oxygen atoms require very large basis sets of plane waves, the size of these systems is intractable with $\mathcal{O}((\#of electons)^3)$ scaling in current methods. Hence there is an imminent need to correct this situation. Fortunately, in most biomolecules, one can identify a few localized active sites and usually only these sites are relevant in elucidating functions of given molecules. Because this implies that the remaining part of the molecule is inert, there is an apparent analogy between the surrounding inactive *back-bones* in these systems and the ionic *cores* in pseudopotential theory. Therefore,

it would appear very sensible to pseudize inactive back-bones, in the same spirit as when one pseudizes atoms. The immediate advantage of modeling the interaction between electrons and back-bones by introducing *molecular* pseudopotentials is that one can reduce the number of electrons by a large amount.

With such a perspective in this dissertation, I have concentrated on extending the territory of applicability of first principles calculations (the theoretical background of which is briefly discussed in chapter 2) toward the realm of molecules and liquids. As a first step in this direction, I describe calculations of hydrogen adsorption on the classic (111)-(7×7) reconstructed surface of Si in chapter 3. The myriad of dangling bond sites on this extremely complex surface offer a unique "laboratory" in which to study atom-surface interactions. As a next step, in chapter 4, I then apply the same theoretical foundation to study the molecular complex $(H_2O)_6^-$. Such clusters of water molecules can be created in fine-mists but, other than their existence, very little is known about their geometric or electronic structures either experimentally or theoretically. By combining state-of-the-art quantum chemical and first-principles density functional techniques, this study not only results in a wide range of new predictions but also helps establish the validity of the first-principles approach to the case of non-solid environments. Finally, in chapter 5, I introduce the concept of a *molecular* pseudopotentials in order to investigate, in a tractable first-principles fashion, the physical and chemical properties of an excess electron migrating through bulk liquid water at room temperature. These calculations successfully reveal, for the very first time, the intricate and microscopic process associated with electron transport in this fundamental system. In addition to the new revelation on the transport mechanism of the excess electron, one should note that the idea of molecular pseudopotentials is successfully implemented in a system of more than 300 atoms, which in particular includes oxygen atoms that must be described by strong pseudopotentials. As a result one can now expect that these kind of molecular pseudopotentials will eventually allow us to simulate *in vitro* experiments.

# Chapter 2

# Theoretical Background of First Principles Calculations

With the advance of huge computational power available in recent years, it is now possible to predict physical and chemical properties of a variety of materials through total energy calculations. This development, in fact, was possible with parallel progress in Kohn-Sham theory and in practical implementations of Pseudopotentials. In this chapter, we will address relevant components in total energy calculations, which are used throughout the projects in following chapters.

## 2.1 Born-Oppenheimer Approximation

To predict the electronic and geometric properties of given materials, we need the power to calculate the total energy and minimize it with respect to electronic and ionic degrees of freedom. Because there is a huge difference in mass between the electrons and nuclei, while the forces on the particles are the same, the electrons can be considered adiabatically following the motions of the nuclei. This approximate separation between electronic and nuclear degrees of freedom in Hilbert space is called the Born-Oppenheimer approximation. In the usual form of this approximation, we need treat only the electrons quantum mechanically. The dynamics of the nuclei can simply be treated with classical mechanics.

## 2.2 Density Functional Theory

Even with the Born-Oppenheimer approximation, it is not easy to calculate the energy of the electron system. It is because of the electron-electron interaction which makes the problem a genuine many-body problem. Only with further simplications, it is practically possible to evaluate some physical quantities. One of the essential simplication comes from so-called Kohn-Sham theory, or Density Functional Theory. Hohenberg and Kohn [1] proved that total energy including the exchange and the correlation of an electron gas is the unique functional of the electron density. The minimum value of the functional is the ground state energy and the density minimizing the functional is the exact one electron ground state density. Then Kohn and Sham [2] showed it is, in principle, possible to map the system of highly-correlated electrons to that of non-interacting electrons under an effective non-local potential.

The generalized Kohn-Sham functional can be written as follows,

$$\begin{aligned} E[\{\psi_n\}] &= \sum_n f_n \int \psi_n^*(\mathbf{r}) \left[\frac{-\hbar^2}{2m}\right] \Delta\psi_n(\mathbf{r})d\mathbf{r} + \int V_{\text{ion}}(\mathbf{r})n(\mathbf{r})d\mathbf{r} \\ &\quad + \frac{e^2}{2}\int \frac{n(\mathbf{r})n(\mathbf{r}')}{|\mathbf{r}-\mathbf{r}'|}d\mathbf{r}' + E_{\text{XC}}[n(\mathbf{r})] + E_{\text{Ion}}(\{\mathbf{R}_I\}) \end{aligned} \tag{2.1}$$

In the functional, $f_n$ is the occupation number of corresponding orbital $\psi_n$, $V_{ion}$ is the total electron-ion interaction potential, $E_{XC}[n(\mathbf{r})]$ is the so called exchange-correlation energy, and $E_{ion}(\{R_I\})$ is the Coulomb energy associated with between ions. Here the electron density is given by

$$n(\mathbf{r}) = \sum_n f_n |\psi_n(\mathbf{r})|^2 \tag{2.2}$$

In the Density Functional Theory, only the minimizing $n(\mathbf{r})$ of the KS functional and the value of the functional for that $n(\mathbf{r})$ have the physical meaning. Therefore, by varying $\psi_n$s, we can obtain following Kohn-Sham equations,

$$\left[\frac{-\hbar^2}{2m}\Delta + V_{\text{Ion}}(\mathbf{r}) + V_{\text{H}}(\mathbf{r}) + V_{\text{XC}}(\mathbf{r})\right]\psi_n(\mathbf{r}) = \varepsilon_n\psi_n(\mathbf{r}) \quad , \tag{2.3}$$

where $\varepsilon_n$ is the Kohn-Sham eigenvalue. The Hartree potential $V_H$ and the exchange-correlation potential $V_{XC}$ are formally given by,

$$\begin{aligned} V_H(\mathbf{r}) &= \frac{\delta E_H[n(\mathbf{r})]}{\delta n(\mathbf{r})} = e^2 \int \frac{n(\mathbf{r}')}{|\mathbf{r}-\mathbf{r}'|} d\mathbf{r}', \\ V_{XC}(\mathbf{r}) &= \frac{\delta E_{XC}[n(\mathbf{r})]}{\delta n(\mathbf{r})} \quad . \end{aligned} \tag{2.4}$$

The Hohenberg-Kohn theorem provides some motivation for using approximate methods to describe the exchange-correlation energy as a function of the electron density. The simplest methods of describing the exchange-correlation energy of an electron system is to use the local-density approximation (LDA) [2], and this approximation is widely used in total energy calculations. In LDA, the exchange-correlation functional is constructed by assuming that the exchange-correlation energy per electron at a point $\mathbf{r}$ in the electron gas is equal to that in a uniform electron gas, $\epsilon_{XC}(n(\mathbf{r}))$, that has the same density as the electron gas at point $\mathbf{r}$. Thus

$$E_{XC}[n] = \int \epsilon_{XC}(n(\mathbf{r}))n(\mathbf{r})d\mathbf{r}, \tag{2.5}$$

and

$$\frac{\delta E_{XC}[n(\mathbf{r})]}{\delta n(\mathbf{r})} = \epsilon_{XC}(n(\mathbf{r})) + \epsilon'_{XC}(n(\mathbf{r}))n(\mathbf{r}). \tag{2.6}$$

There are several parameterizations [2, 3, 4, 5, 6] for local exchange-correlation energy. These are all interpolations to link values in various density regions. Specially Perdew and Zunger's parameterization [6] has been widely and quite successfully used. However, even though LDA has been very successful (one of the reason it is very successful can be attributed to the fact that it gives the correct sum rule for the exchange-correlation hole [15, 16, 17].), it has been seen that some improvement to LDA is necessary for systems where intermediate bonds like hydrogen bonding are important. Gradient Correction [18] is one of those attempts to improve LDA. In

gradient correction, the exchange correlation functional is written as follows,

$$E_{\mathrm{XC}}[n] = \int \epsilon_{\mathrm{XC}}(n(\mathbf{r}), \nabla n(\mathbf{r}))n(\mathbf{r})d\mathbf{r} \quad , \tag{2.7}$$

By having $\nabla n(\mathbf{r})$ in the functional, gradient corrected functional tends to give better results for systems which have either very localized states or very weak bonds. In recent years, a few promising forms of gradient correction [7, 8, 9, 10] are proposed. We expect that there would be an outstanding one after several years' field test.

## 2.3 Periodic Supercells

In many cases, the system in our interest has a natural periodicity. In such a case, KS equations can be labelled by Bloch's Theorem. Bloch's Theorem says that when the system has a periodicity, the eigenstates of KS Hamiltonian can be decomposed into a cell-periodic part and a wavelike modulation,

$$\psi_{n,\mathbf{k}}(\mathbf{r}) = e^{i\mathbf{k}\cdot\mathbf{r}} u_{n,\mathbf{k}}(\mathbf{r}) \quad . \tag{2.8}$$

Since the cell-periodic function $\mathrm{u_{n,k}}(\mathbf{r})$ can be expanded in Fourier space, the Eq. 2.8 can be rewritten as

$$\psi_{n,\mathbf{k}}(\mathbf{r}) = \sum_{\mathbf{G}} c_{n,\mathbf{k}+\mathbf{G}} e^{i(\mathbf{k}+\mathbf{G})\cdot\mathbf{r}} \quad . \tag{2.9}$$

where $\mathbf{G}$ are the reciprocal lattice vectors defined by $\mathbf{G}\cdot\mathbf{l}/2\pi \in \mathbb{Z}$, and $\mathbf{l}$ is a lattice vector of the crystal

However, in principle, we need to evaluate $\psi_{\mathrm{n,k}}$ at infinite number of $\mathbf{k}$ points to construct KS Hamiltonian. Specifically, in evaluating Eq. 2.2, the integration should be done all over the Brillouin Zone (BZ). One insight in this problem is the observation that $\psi_{\mathbf{k}}$ at a point $\mathbf{k}$ can be used as a representation for the neighborhood. Methods are devised for obtaining very accurate representation by calculating the electron states at special sets of $\mathbf{k}$ points in BZ [19]. Therefore we can approximate

the integration in BZ as follows,

$$\int_{\mathrm{BZ}} \frac{d\mathbf{k}}{\Omega_{\mathrm{BZ}}} \rightarrow \sum_{\mathbf{k}}^{m} w_{\mathbf{k}}. \tag{2.10}$$

where $w_{\mathbf{k}}$ is the weighting factor for $\mathbf{k}$.

Even though there are infinite number of reciprocal lattice vectors, typically the coefficients $c_{\mathrm{n},\mathbf{k}+\mathbf{G}}$ with small kinetic energy $\frac{\hbar^2}{2m}|\mathbf{k}+\mathbf{G}|^2$ are more important than those with large kinetic energy. Thus we can restrict the plane-wave basis just to include ones that have kinetic energies less than a given cutoff energy. In other words, at each $\mathbf{k}$ point, we allow $\mathbf{G}$ which satisfies

$$\frac{\hbar^2}{2m}|\mathbf{k}+\mathbf{G}|^2 < E_{\mathrm{cut}} \quad . \tag{2.11}$$

Cutoff energies can be chosen such that relevant quantities are converged within a tolerance level. The finite $\mathbf{k}$ sampling can make a discontinuity problem with basis truncation as we increase the cutoff energy even though dense enough $\mathbf{k}$ points tend to average out this discontinuity in the tolerance level. It is shown that this discontinuity can be handled by applying correction factors [20]. Once we have a finite plane basis $\{\mathbf{G}\}$, the Eq. 2.3 becomes a secular equation

$$\begin{aligned}\sum_{\mathbf{G}'} \left[\frac{-\hbar^2}{2m}|\mathbf{k}+\mathbf{G}|^2 \delta_{\mathbf{G}\mathbf{G}'} + V_{\mathrm{ion}}(\mathbf{G}-\mathbf{G}') + V_{\mathrm{H}}(\mathbf{G}-\mathbf{G}') + V_{\mathrm{XC}}(\mathbf{G}-\mathbf{G}')\right] c_{n,\mathbf{k}+\mathbf{G}'} \\ = \varepsilon_n c_{n,\mathbf{k}+\mathbf{G}'}.\end{aligned} \tag{2.12}$$

So for periodic systems, Eq. 2.12 is the finite size master equation we have to solve. But for non-periodic systems, we cannot apply Bloch's theorem so that we do not have a finite size secular equation as we do in periodic systems. The supercell geometry can be used in such occasions. The idea is that the artificial periodicity becomes irrelevant when the cell size grows. Therefore, for large enough cell the size of which depends on the nature of the original system, the calculated physical quantities can be used to answer questions about the original systems.

## 2.4 Pseudopotentials

### 2.4.1 Pseudopotential Approximation

Although we have seen it is possible to have finite size secular equation, the typical energy cutoff will be too high if we perform an all electron calculations. That is because the core electrons are tightly bounded to nuclei and the valence electrons rapidly oscillate in the core region to maintain their orthogonality to core electrons. Pseudopotential Approximations [11, 12, 13] (PA) start from the well known fact that most of physical and chemical properties of solids solely depend on the valence electrons. Thus in PA, we assume that core electrons are frozen in their atomic orbitals. In addition, inside of core region defined by frozen core, we modify ionic potentials in such a way that valence electron wavefunctions have the same scattering properties outside the core. Then the pseudo valence electron orbitals do not have rapidly oscillating behavior inside the core while maintaining its physical bonding properties. Since valence electrons in different angular momentum states see the core in different ways, there cannot be a unique modification to all angular momentum states. Thus the general form of pseudopotential is

$$v^{\mathrm{ps}} = \sum_{l,m} v_l \left|lm\right\rangle \left\langle lm\right| . \tag{2.13}$$

where $|lm\rangle$ are the spherical harmonics and $\mathrm{v}_l$ is the pseudopotential for angular momentum $l$.

### 2.4.2 Norm Conservation

After the first introduction of the pseudopotential by Fermi [21] in 1934 to study the high lying atomic states and the OPW type derivation of Phillips-Kleinman cancellation theorem [22], diverse variations [23, 24, 25, 26, 27, 28] of the pseudopotential method have been developed including the model pseudopotential methods, the empirical pseudopotential methods, and the self-consistent pseudopotential methods.

Modern pseudopotentials can be termed as *ab initio norm conserving* pseudopotentials. These potentials share the following features:

1. The real and pseudo atom have the same valence eigenvalues for a set of electron configuration, known as the reference configurations.

2. The pseudowavefunction does not have core oscillation and is identical to the real valence wavefunction outside the pseudo core.

3. The pseudo-charge contained inside the pseudo core is identical to the real electron charge in the region.

Specially, the condition 3 is critical in *transferability*, the property which ensures the pseudopotentials can describe the scattering due to the ion in a variety of atomic environments [29]. This comes from the following identity which is related to the Friedel sum rule,

$$-\left[\frac{\partial}{\partial\varepsilon}\frac{\partial}{\partial r}\ln R_l(r)\right]_{r=r_0,\varepsilon=\varepsilon_l} = \frac{1}{r_0^2 R_l^2(r_0)}\int_0^{r_0}\left[rR_l(r)\right]^2 dr, \tag{2.14}$$

where $R_l(r)$ is the radial wavefuntion and $\varepsilon_l$ is the eigenenergy for the angular momentum state $l$ and $r \geq r_{core}$. That is because Eq. 2.14 relates the energy dependence of phase shift (logarithmic derivative) to the charge inside core region.

### 2.4.3 Separable Nonlocal Pseudopotential

Eq. 2.13 can be rewritten as

$$v^{\mathrm{ps}} = v_{\mathrm{local}} + \sum_{l,m} \Delta v_l \left|lm\right\rangle \left\langle lm\right| \quad , \tag{2.15}$$

where $\Delta v_l = v_l - v_{\mathrm{local}}$. Since Eq. 2.15 is not a separable form, the operational cost in evaluating matrix multiplication is $\mathcal{O}(N_{pw}^2)$ where $N_{pw}$ is the number of plane-wave basis. When compared with $\mathcal{O}(N_{pw} ln N_{pw})$ scaling for local potentials, it is very desirable to have a separable form which can scale linearly in $N_{pw}$. Kleinman and

Bylander [30] first suggested a form of fully nonlocal separable pseudopotential:

$$\Delta v^{\mathrm{KB}} = \sum_{l,m} \frac{\Delta v_l \, u_l \, |lm\rangle \, \langle lm| \, \Delta v_l \, u_l}{\langle u_l | \Delta v_l | u_l \rangle} \quad , \tag{2.16}$$

where $u_l$ are the wavefunctions of the pseudoatoms. One pitfall in using KB factorization is that there might be ghost states. This is because one cannot obtain KB pseudopotentials by applying transformation on the semi-local pseudopotentials in Eq. 2.15. Therefore, a full analysis on the possible ghost states [31, 32] should be done before the use of a KB factorized pseudopotential.

## 2.5 Ion-Ion Interactions

It is extremely difficult to compute the Coulomb energy of the ionic system using a direct real space summation because the coulomb interaction is long ranged. The Coulomb interaction is also long ranged in reciprocal space, so the the problem is not solved just by performing the summation in reciprocal space. Ewald [33] developed a rapidly convergent method for performing Coulomb summations over periodic lattices. His method is based on the following identity:

$$\begin{aligned} \sum_{\mathbf{l}} \frac{1}{|\mathbf{R_1} + \mathbf{l} - \mathbf{R_2}|} = \frac{2}{\sqrt{\pi}} \sum_{\mathbf{l}} \int_{\eta}^{\infty} exp\left[ - |\mathbf{R_1} + \mathbf{l} - \mathbf{R_2}|^2 \, \rho^2 \right] d\rho \\ + \frac{2\pi}{\Omega} \sum_{\mathbf{G}} \int_{0}^{\eta} exp\left[ -\frac{|\mathbf{G}|^2}{4\rho^2} \right] \times exp\left[ i(\mathbf{R_1} - \mathbf{R_2}) \cdot \mathbf{G} \right] \frac{1}{\rho^3} d\rho, \end{aligned} \tag{2.17}$$

where $\mathbf{l}$ are lattice vectors, $\mathbf{G}$ are reciprocal vectors, and $\Omega$ is the volume of the unit cell. This identity provides a method for rewriting the lattice summation for the Coulomb energy due to the interaction between an ion position at $\mathbf{R_2}$ and an array of atoms positioned at the points $\mathbf{R_1} + \mathbf{l}$. The identity holds for all positive values of $\eta$. At first sight, the infinite Coulomb summation on the left hand side of Eq. 2.17 has been replaced by two infinite summations, one over lattice vectors and the other over reciprocal lattice vectors. However, if one chooses an appropriate value of $\eta$ the two summations become rapidly convergent in their respective spaces. The the real and

reciprocal space summation can be computed only with a few lattice vectors and a few reciprocal lattice vectors. As mentioned in the preceding section, the contribution to the total energy from the electro-ion, ion-ion, and electron-electron interactions at $\mathbf{G} = 0$ cancel exactly, and so the $\mathbf{G} = 0$ contribution to the Coulomb energy of the ionic system must be removed in order to compute the correct total energy. In the Ewald summations the $\mathbf{G} = 0$ contribution to the Coulomb energy has been divided between the real space and the reciprocal space summations, so that it is not sufficient simply to omit the $\mathbf{G} = 0$ term in the reciprocal space Ewald summation. The $\mathbf{G} = 0$ term in the reciprocal space summation should be omitted and two terms added to the Ewald energy to give the correct total energy. The correct form [34] for the total energy is

$$\begin{aligned} E_{\text{ion}} &= \frac{1}{2}\sum_{I,J} Z_I Z_J e^2 \{\sum_{l} \frac{\text{erfc}\left(\eta\left|\mathbf{R_1}+\mathbf{l}-\mathbf{R_2}\right|\right)}{\left|\mathbf{R_1}+\mathbf{l}-\mathbf{R_2}\right|} - \frac{2\eta}{\sqrt{\rho}}\delta_{IJ} \\ &\quad + \frac{4\pi}{\Omega}\sum_{\mathbf{G}\neq 0} \frac{1}{|\mathbf{G}|^2} exp\left[-\frac{|\mathbf{G}|^2}{4\rho^2}\right] \times cos\left[(\mathbf{R_1}-\mathbf{R_2})\cdot\mathbf{G}\right] - \frac{\pi}{\eta^2\Omega}\}, \end{aligned} \quad (2.18)$$

where $Z_I$ and $Z_J$ are the valences of ions I and J, respectively, and erfc is the complementary error function. An ion does not interact with its own Coulomb charge, so the $l = 0$ term must be omitted from the real space summation when $I = J$.

## 2.6 Iterative Methods

Modern methods in solving secular equations are mostly based on Operator viewpoint of the Hamiltonian while direct diagonalization methods emphasize individual matrix elements. The common features in modern indirect diagonalization methods are as follows,

1. They keep the track of low lying eigen-states in Hilbert space.
2. They starts from a reasonable starting set of low lying eigen-states which still carries the symmetry of the given system.

3. They updates states using correction vectors, $(H-\varepsilon_n^{old})\psi_n^{old}$, which are obtained by multiplying existing vectors to the Hamiltonian.

These features are very important two-folds. The first is that we do not have to put the Hamiltonian matrix in the memory and the second is that we can control the accuracy of the final eigenstates by increasing the number of iterations.. At this moment, there are a few methods widely used for total energy calculations. Among them, we have mainly used two methods: Car-Parinello Molecular Dynamics [35] and Conjugate Gradient Methods [36]. The details of two methods are well documented in the literature [36].

## 2.7 Ion Dynamics

The forces on ion I, $\mathbf{f}_I$, is given by

$$\mathbf{f}_I = -\frac{dE}{d\mathbf{R}_I} = -\frac{\partial E}{\partial \mathbf{R}_I}. \tag{2.19}$$

The reason we can replace the total derivative with the partial derivative is from Hellmann-Feynman Theorem [37, 38]. Because the errors in forces are linearly proportional to errors in wavefunctions, one should ensure that forces are well converged in ion dynamics calculations. In integrating ion trajectories, Verlet algorithms are conventionally used. However, just for structural minimization, one does not need very accurate forces at all steps as long as energy decreases in a reasonable way.

# Chapter 3

# Hydrogen Adsorption on Si(111) Surface

First-principles total energy pseudopotential calculations are performed to investigate the adsorption interaction of a hydrogen atom with dangling bonds on the Si(111)-$(7 \times 7)$ surface. The binding energies for adsorption of H at the adatom, rest atom, and corner hole sites, are calculated to be 2.9 eV, 3.2 eV, and 3.5 eV respectively. Spectral analysis of the electronic states shows that *non-local* changes of chemical reactivity are induced by *charge transfer* upon H adsorption. It is found that H adsorption on the adatoms or rest atoms induces a charge transfer onto the Si-H bond and a shift in energy of the remaining dangling bond states. Adsorption on the corner hole, however, does not involve any charge transfer. The relationship between charge transfer and binding energies is discussed.

## 3.1 Introduction

First-principles study of the adsorption process on a surface is important for understanding microscopic processes on the surface, such as the initial stages of epitaxial growth of thin films, initial stages of surface corrosion, and surface catalysis [39]. The interaction of adsorbed atoms with each chemically active site on the surface induces a change of the local electronic structure as well as a relaxation of the lo-

cal geometry specific to the site. Most experiments provide only limited information about the adsorption process, averaging over a large number of active sites. The study of "atom-resolved surface chemistry using scanning tunneling microscopy" has revealed large differences in electronic spectra at different surface sites [40]. The local properties obtained by first-principles studies can provide complementary microscopic information for understanding the microscopic aspects of the adsorption process.

Adsorption on semiconductor surfaces has been studied extensively because of the technological importance of the surfaces in electronic device fabrication. Specifically, adsorption on the Si(111) surface has been a challenging problem because of the complexity of the stable reconstruction geometry [41]. First-principles studies of the intrinsic $(7 \times 7)$ surface reconstruction became possible only recently with the help of rapid developments in massively parallel processors (MPP) [42, 43]. The adsorption problem is more challenging than the reconstruction problem for two reasons: First, the strong potential of adsorbed atoms such as H increases considerably the number of basis functions needed to describe the system. Second, it is necessary to investigate several different adsorption sites in order to fully understand the physics and chemistry involved.

The equilibrium structure of the Si(111) surface at temperatures below 870 $^{o}$C consists of a $(7 \times 7)$ reconstruction in which the surface atoms rearrange to lower the surface energy. The Takayanagi dimer-adatom-stacking fault (DAS) model is now generally accepted as the model that correctly describes this reconstruction [41]. A ball-and-stick model of the DAS $(7 \times 7)$ reconstruction is shown in Fig. 3-1. The $(7 \times 7)$ surface unit cell is indicated by the broken lines in the top panel of Fig. 3-1. The unit cell consists of two triangles separated by three dimers. The left triangle has a stacking fault between the third layer and the fourth layer as shown in the bottom panel of Fig. 3-1. Each triangle has six adatoms and three rest atoms indicated respectively as large black dots and gray dots in Fig. 3-1. The corner hole atoms are indicated as small black dots at the vertices of the unit cell.

There are nineteen chemically active sites on each surface unit cell: twelve adatom dangling bonds, six rest atom dangling bonds, and one corner hole dangling bond.

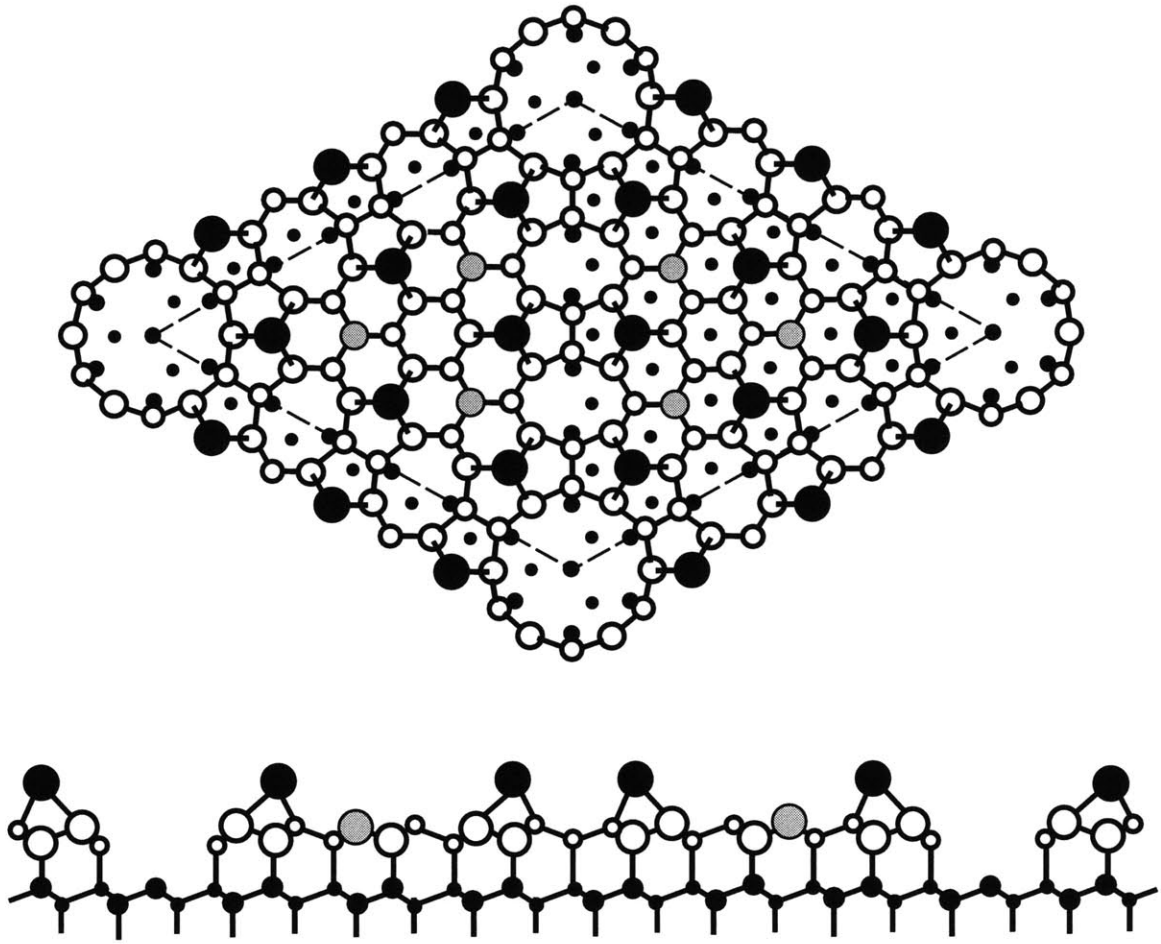

Figure 3-1: Ball-and stick model of the Si(111)-(7 $\times$ 7) surface. Top panel shows the top view, and bottom panel shows side view along the long diagonal of the unit cell.

Analysis of local chemical reactivity based on first-principles calculations [44] has shown that these dangling bonds have different capacities to donate and accept electrons and, consequently, different reactivities with various reactants. Specifically, the surface charge donor capacity is proportional to the amount of electrons in dangling bonds so that the donor capacity (and chemical reactivity) follows the order: corner hole > rest atoms > adatoms.

In this work, we choose atomic hydrogen as a prototypical strongly electronegative reactant and investigate hydrogen adsorption on the Si(111)-(7 × 7) surface. The calculated adsorption energies are consistent with the analysis of local chemical reactivity and the experimental observation that the corner hole is the most active site for hydrogen adsorption. In section 3.2, we describe the method of first-principles calculation. In sections 3.3, 3.4, and 3.5, we discuss the details of the microscopic structural and electronic changes induced by hydrogen adsorption.

## 3.2 Computational Method

The Si(111)-(7 × 7) surface is modeled by a five layer slab in the supercell of $(26.6\text{Å})^2$ ×16.5Å which includes one (7 × 7) surface unit and 10Å vacuum between the slabs. These five layers are shown in the bottom panel of Fig. 3-1 in the ball-and-stick model representation. The top side of the slab is used to construct the DAS (7 × 7) reconstruction, and the bottom layer silicon atoms are fixed in the bulk positions. The dangling bonds of the bottom layer silicon atoms are saturated by hydrogen atoms (which are not shown in Fig. 3-1).

For the minimization of the electronic energy functional at each ionic configuration, the *ab initio* molecular dynamics scheme implemented on the MPP CM-5 [36, 45] is used. The ion positions are relaxed according to the Hellmann-Feynman forces calculated from the minimized electron wave functions. At the fully relaxed configuration of the intrinsic (7 × 7) surface, the Hellmann-Feynman forces on the silicon atoms are smaller than 0.1 eV/Å. Electron wave functions are expanded in a plane-wave basis with 11.5 Ry cutoff energy which corresponds to about 50,000 basis

functions. The Brillouin zone sampling is approximated by the $\Gamma$ point. Optimized pseudopotentials [27] for the silicon atom and the hydrogen atom are used in the Kleinman-Bylander separable form [30].

Hydrogen adsorption calculations were performed for three representative surface dangling bond sites: the corner adatom on the unfaulted side, the rest atom on the unfaulted side, and the corner hole atom. The quality of the pseudopotentials and energy cutoff was tested by comparison with $SiH_4$ and hydrogen adsorption on the Si(111)-$(1 \times 1)$ surface. The optimized geometry of $SiH_4$ has a Si-H bond length 2.7% larger than the experimental bond length of 1.48 Å. The hydrogen adsorption energies on the Si(111)-$(1 \times 1)$ surface were calculated both for the surface with a stacking fault and without a stacking fault, and were found to be 3.50 eV and 3.46 eV respectively. These values are in good agreement with the hydrogen adsorption energy (3.6 eV) calculated independently by Van de Walle using a similar computational scheme [46]. Note that the stacking fault introduces only 0.04 eV difference in the adsorption energy.

First, a hydrogen atom was placed 1.5 Å above a corner adatom on the unfaulted side, and the geometry of the surface and the adsorbed hydrogen was relaxed. This procedure was repeated with the hydrogen atom above a rest atom on the unfaulted side and with the hydrogen atom above a corner hole atom. Fig. 3-2 shows the total valence charge density cross sections along the long diagonal of the unit cell. From top to bottom the intrinsic surface, the surface with a hydrogen atom on the adatom, the surface with a hydrogen atom on the rest atom, and the surface with a hydrogen atom on the corner hole atom are shown. The covalent bonds between the three Si sites and the adsorbed hydrogens are clearly visible as white dots on the corresponding surface atoms.

## 3.3 Adsorption Energy and Geometry

The adsorption energy is calculated from the difference of the total energies of two separate calculations: one with a hydrogen atom adsorbed on a binding site and one

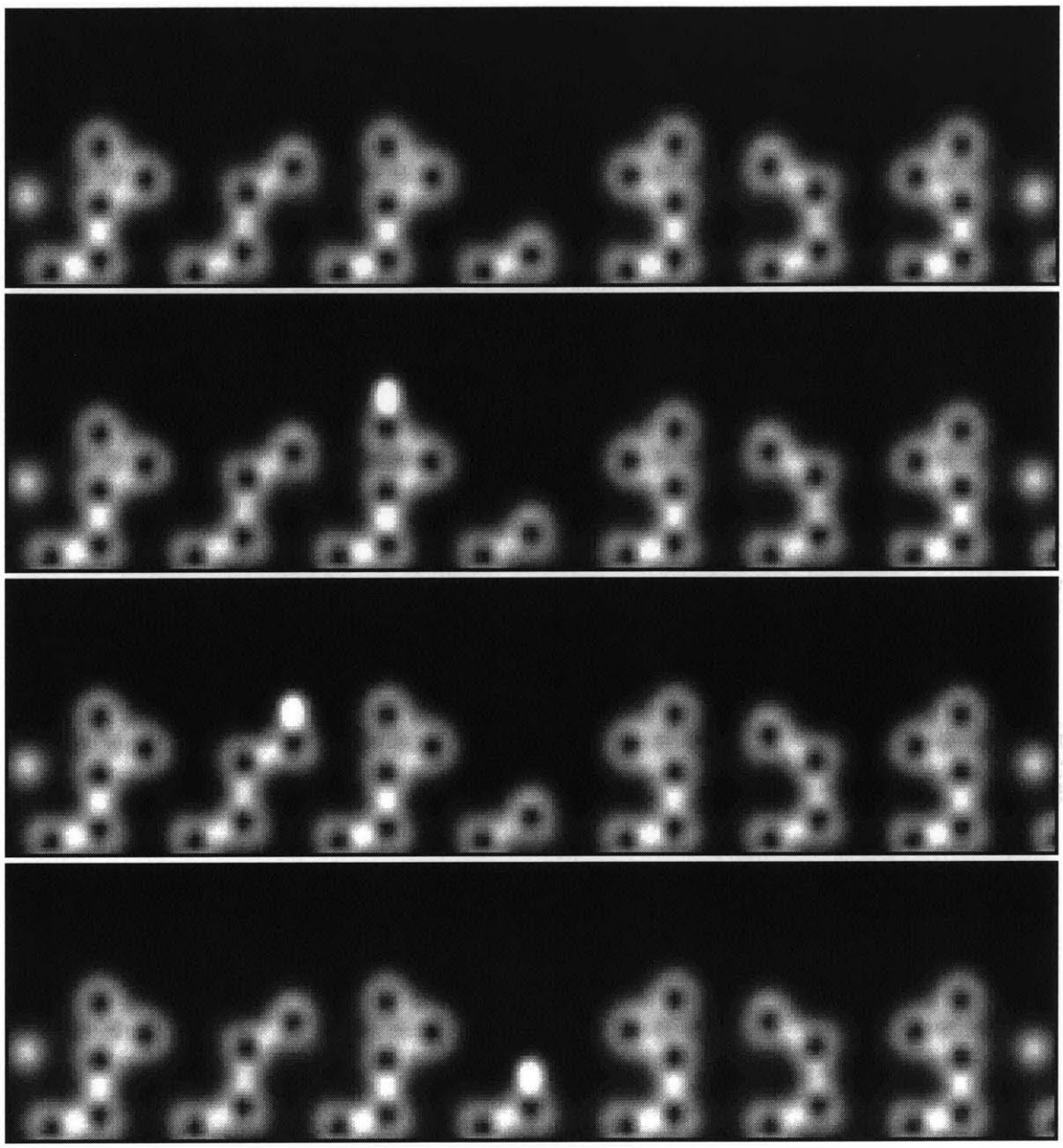

Figure 3-2: Plots of the total valence charge density in a plane perpendicular to the surface along the long diagonal. From top panel to bottom panel, each panel corresponds to the intrinsic surface, the surface with hydrogen on adatom, the surface with hydrogen on rest atom, and the surface with hydrogen on corner hole atom.

with a hydrogen atom fixed in the middle of the vacuum separated from the slabs by 5Å. The calculated adsorption energies are 2.9 eV, 3.2 eV, and 3.5 eV for the hydrogen atom adsorbed on the adatom, the rest atom, and the corner hole atom respectively. These energies are smaller than the hydrogen adsorption energy (3.5 eV) on the Si(111)-(1 × 1) surface. Note that because of the surface periodicity, one hydrogen atom per unit cell of the (1×1) surface corresponds to one monolayer (1ML) coverage whereas one hydrogen atom per unit cell of the (7 × 7) surface corresponds to 0.02ML coverage.

Figs. 3-3, 3-4, and 3-5 show the changes of the local geometries induced by the adsorbed hydrogen atom. The H-Si bond lengths are 1.538 Å, 1.545 Å, and 1.541 Å for the adatom, the rest atom, and the corner hole sites respectively. These bond lengths are very close to the Si-H bond length (1.54 Å) on the Si(111)-(1×1) surface [47]. The differences in bond lengths are small, but significant compared to the typical errors in the bond lengths obtained by the calculations (0.001 Å). Typical errors can be seen from the difference between bond lengths which should be identical by symmetry (*e.g.*, bonds 1-3 and 1-4 in Fig. 3-3, 1-2 and 1-3 in Fig. 3-4, and 1-2, 1-3, and 1-4 in Fig. 3-5). The different Si-H bond lengths, and consequently bonding strengths, cannot explain the large differences in the adsorption energies: for comparison, the results from the $SiH_4$ calculation show a change of only 0.01 eV in the energy for a change of 0.01 Å in the Si-H bond length. Therefore, the large differences of the adsorption energies are resulting either from the relaxation of the (7 × 7) surface geometry or from the changes of electronic structure induced by hydrogen adsorption.

Fig. 3-3 shows that the hydrogen saturation of the adatom dangling bond decreases the adatom backbond length by 0.02-0.03 Å, the three next layer bonds (2-5, 3-5, and 4-5) by 0.02 Å, and the bond 5-6 by 0.04 Å. Fig. 3-4 shows that the hydrogen saturation of the rest atom dangling bond decreases the length of three bonds (1-2, 1-3, and 1-4) by about 0.02 Å, while the next layer bond length changes are negligible. Fig. 3-5 shows a very small change of bond length induced by the hydrogen adsorption. An estimate of the energies involved in these distortions can be obtained from the calculations of Ref. [47], giving about 0.05 eV. Thus, these changes

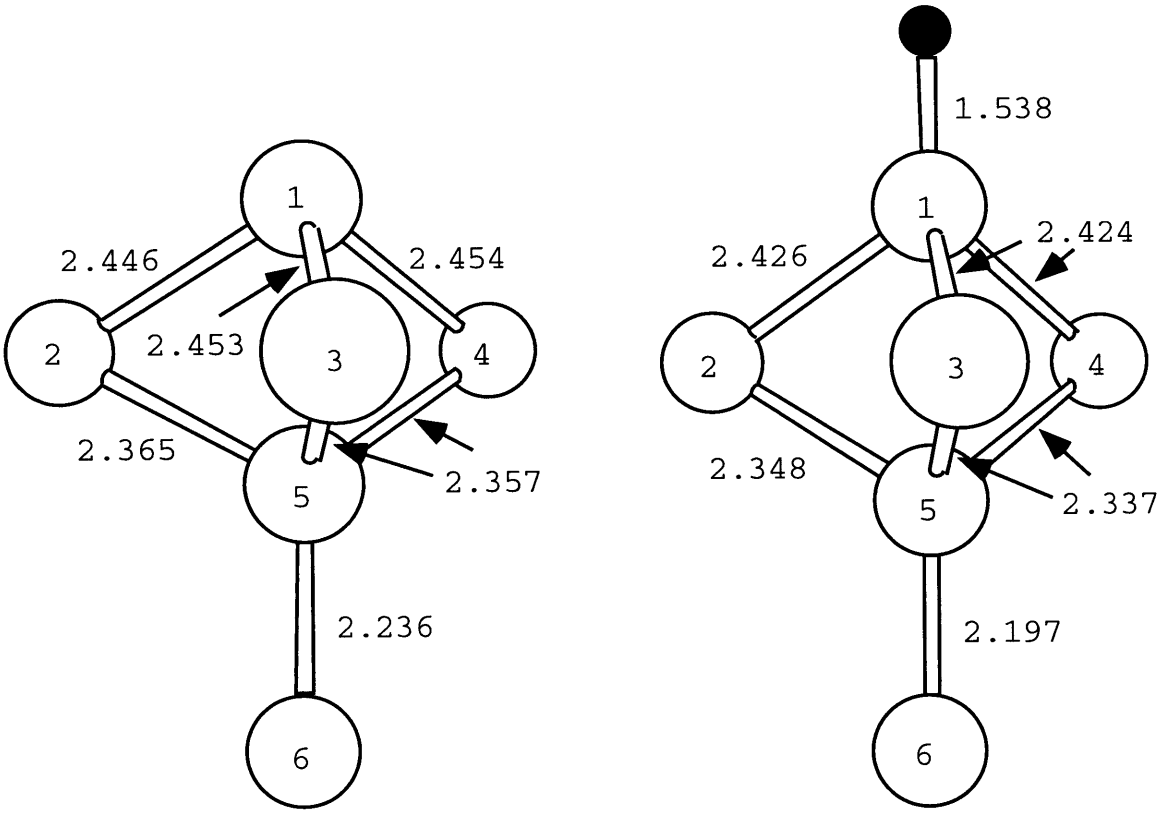


Figure 3-3: Ball-and-stick model representation of the change of local geometry of the adatom induced by hydrogen adsorption.

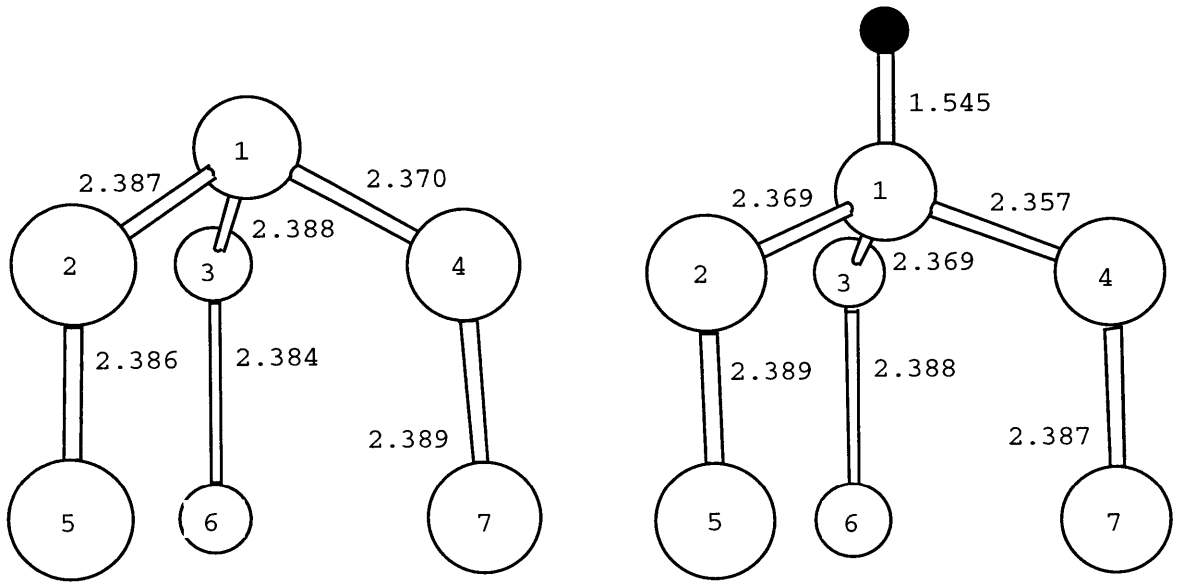


Figure 3-4: Ball-and-stick model representation of the change of local geometry of the rest atom induced by hydrogen adsorption.

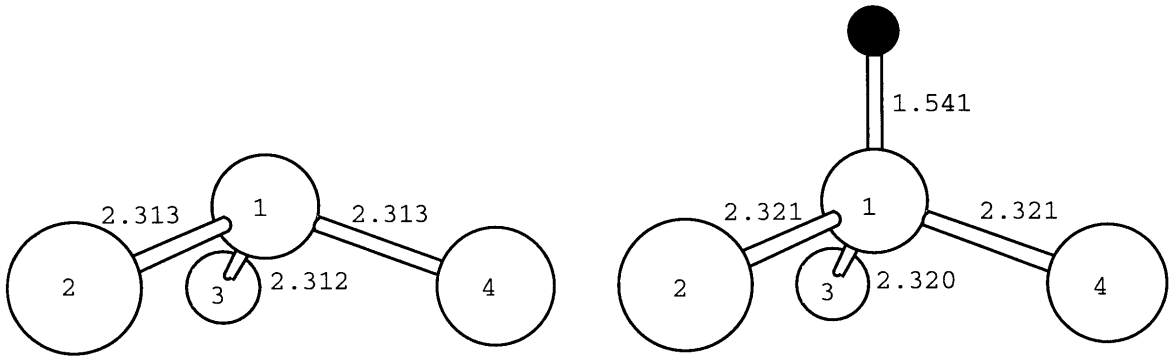


Figure 3-5: Ball-and-stick model representation of the change of local geometry of the corner hole atom induced by hydrogen adsorption.

of geometries are not large enough to explain the significant differences in adsorption energy. Consequently, the electronic structure effect is crucial in understanding the adsorption energies as we discuss in the next section.

## 3.4 Variation in Electronic Structure

The changes of the surface electronic structure by hydrogen adsorption are illustrated in Figs. 3-6, 3-7, 3-8, and 3-9 with the same cross section of the charge densities as in Fig. 3-2 for the occupied electronic states in the specific energy ranges. Figs. 3-6, 3-7, 3-8, and 3-9 are, respectively, for the intrinsic surface, the surface with a hydrogen atom on the adatom, the surface with a hydrogen atom on the rest atom, and the surface with a hydrogen atom on the corner hole atom. The Fermi energy changes slightly from -0.16 eV for Fig. 3-6 to -0.13 eV for Fig. 3-7, -0.09 eV for Fig. 3-8, and -0.06 eV for Fig. 3-9.

The top panel of Fig. 3-6 shows the ball-and-stick model of the intrinsic surface along the long diagonal. In this and the following figures, *a, r, c,* and *H* indicate the adatom, the rest atom, the corner hole atom, and the hydrogen atom respectively. The second panel shows four adatom dangling bonds (from left to right, the center adatom and the corner adatom on the unfaulted side, and the corner adatom and the center adatom on the faulted side), two rest atom dangling bonds, and one corner hole dangling bond in the lower center of the panels. Note that the adatom dangling bonds are also present in the seventh panel (-2.5 eV to -3.0 eV) with larger charge densities in the dangling bonds. The third panel shows the two dangling bonds of the rest atoms: the left on the unfaulted side and the right on the faulted side. The fourth and fifth panels show the adatom backbonds, and the next layer bonds. The sixth panel shows more adatom backbonds (one of them is indicated by an arrow) and the surface dimer bonds at the left and right ends of the panel. The seventh panel shows quite strong covalent bonds between the adatoms and the atoms right below them. The eighth panel shows the difference between the faulted and unfaulted sides: the bonds at the stacking fault on the right side are weaker than the normal bonds

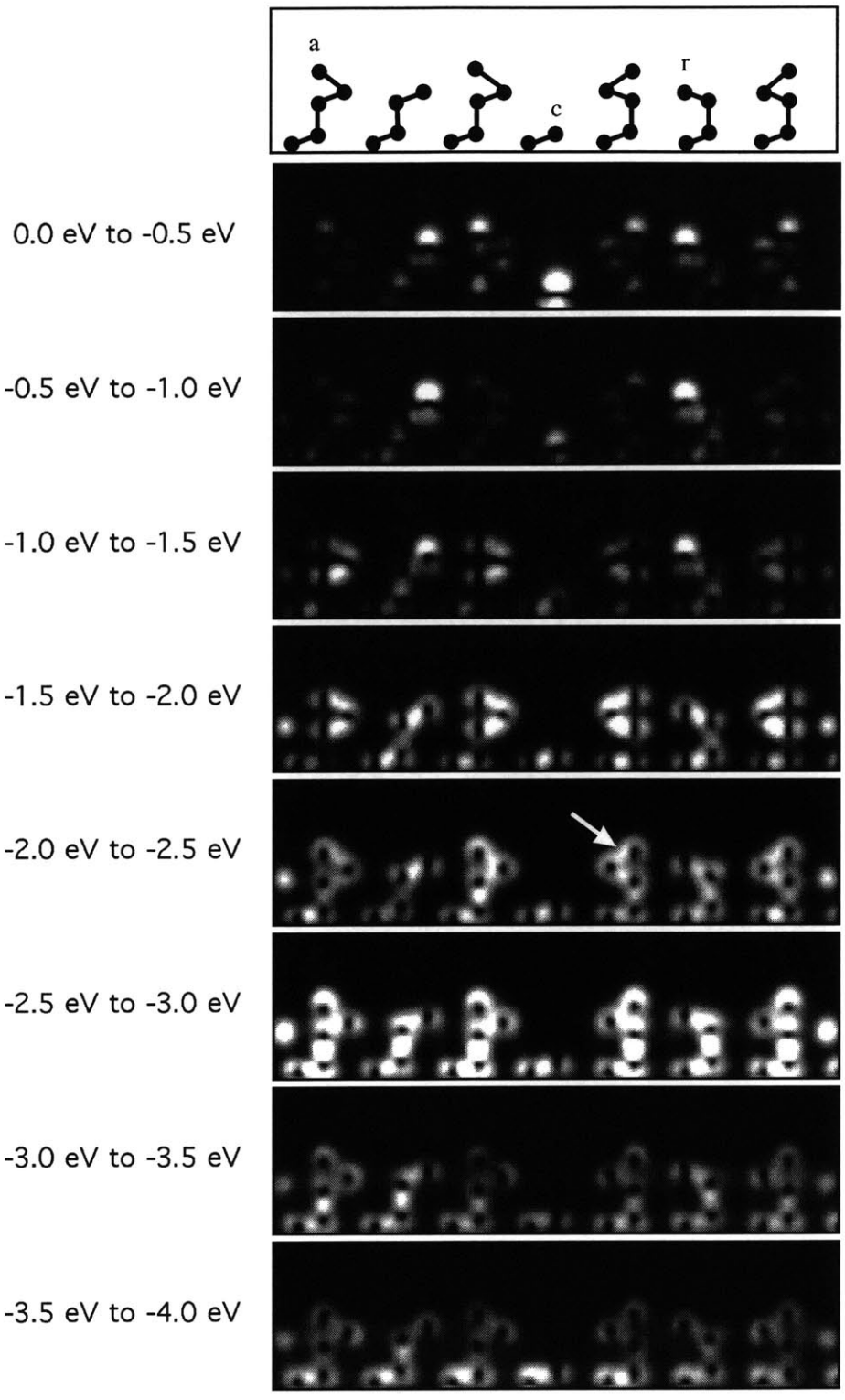


Figure 3-6: Plots of the valence charge density in the specified energy ranges for the intrinsic surface. The cross sections are in the same plane as Fig. 3-2. Top panel shows the ball-and-stick model representation of the atoms in the plane.

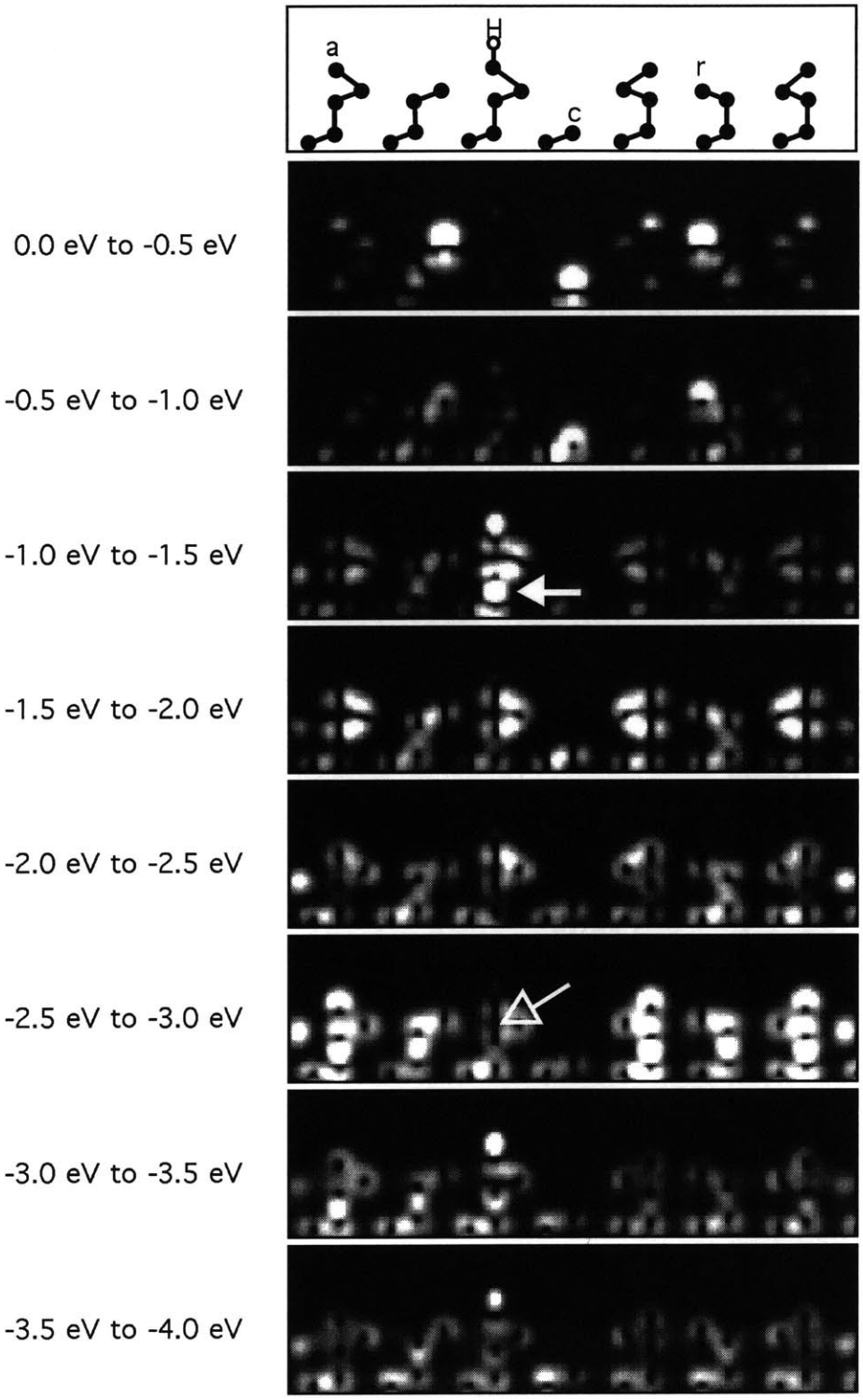


Figure 3-7: Plots of the valence charge density in the specified energy ranges for the surface with hydrogen on adatom using the same convention as Fig. 3-6.

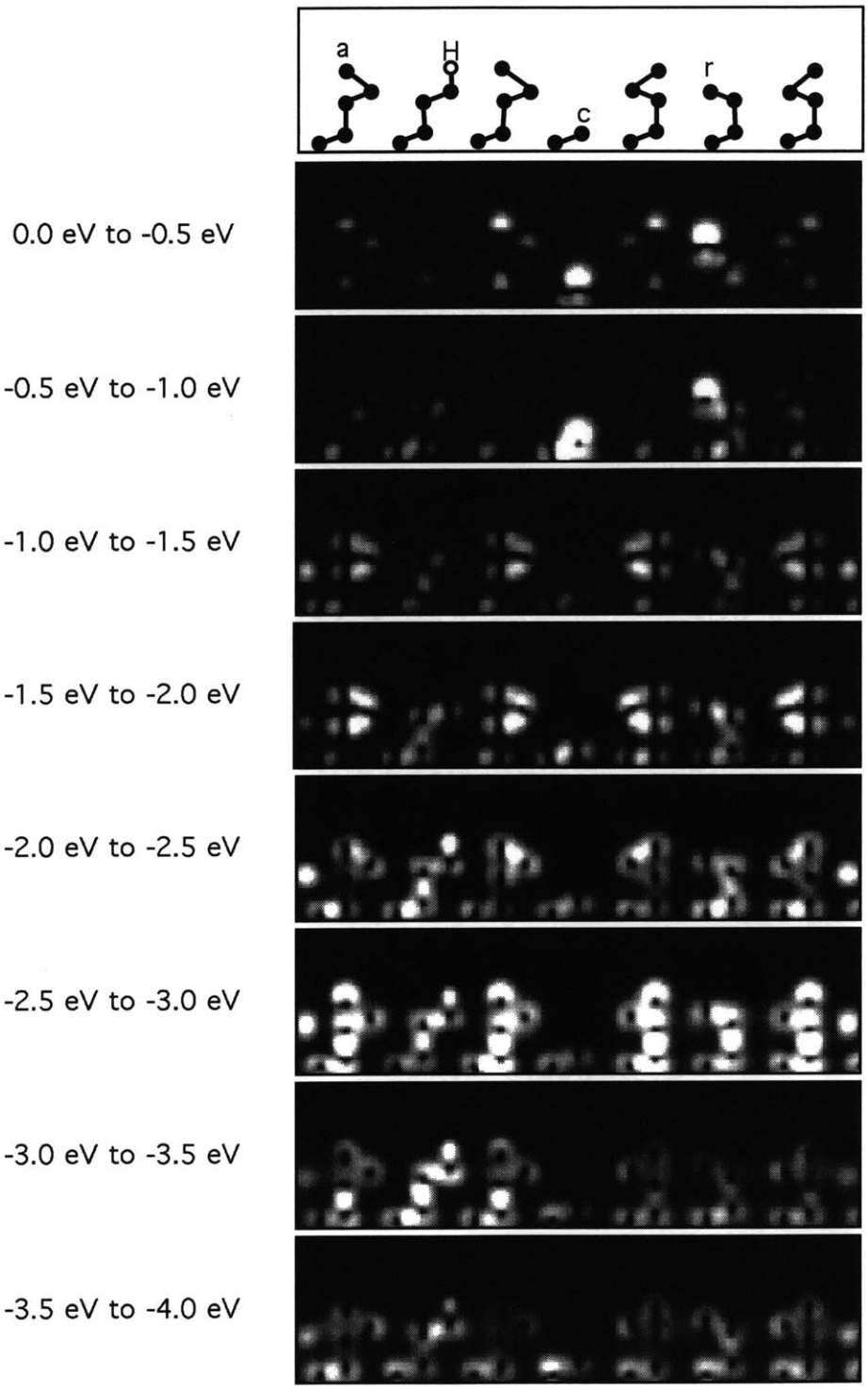


Figure 3-8: Plots of the valence charge density in the specified energy ranges for the surface with hydrogen on rest atom using the same convention as Fig. 3-6.

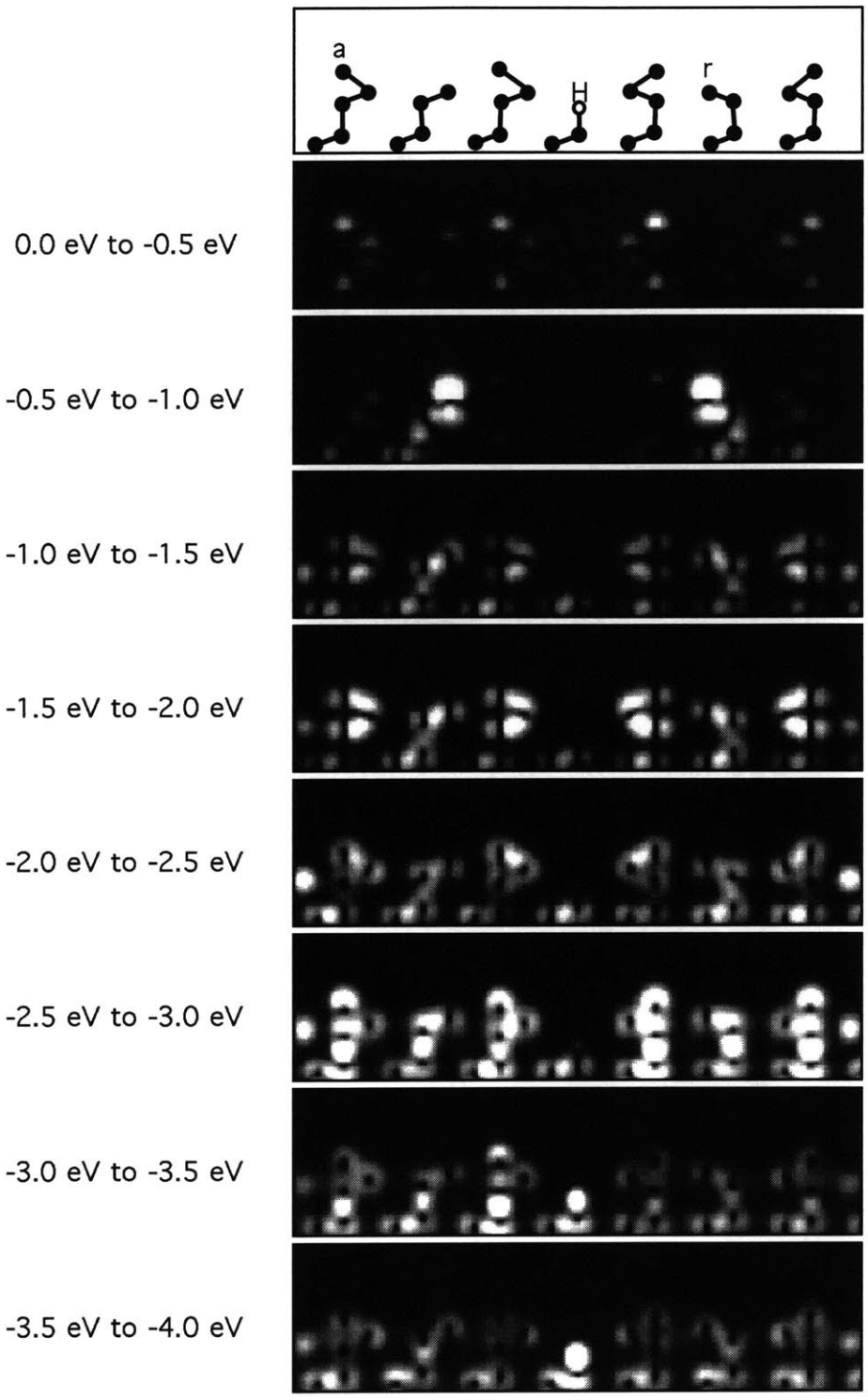


Figure 3-9: Plots of the valence charge density in the specified energy ranges for the surface with hydrogen on corner hole atom using the same convention as Fig. 3-6.

at the left side. The ninth panel shows silicon bonds without specific characteristics.

Fig. 3-7 shows the charge density cross section spectra in the presence of the hydrogen atom on the second adatom from the left, *i.e.*, the corner adatom on the unfaulted side as indicated in the top panel. The spectra of Fig. 3-7 show very striking changes from those of Fig. 3-6: the dangling bond state of the hydrogen-saturated adatom is lowered in energy, from the range [0.0 eV, -0.5 eV] to the range [-1.0 eV, -1.5 eV] and from the range [-2.5 eV, -3.0 eV] to the range [-3.0 eV, -4.0 eV]. The dangling bond states of the rest atoms are raised in energy from the range [-0.5 eV, -1.0 eV] to the range [0.0 eV, -0.5 eV]. Finally, the dangling bond state of the corner hole atom is lowered in energy from the range [0.0 eV, -0.5 eV] to the range [0.0 eV, -1.0 eV]. The fourth panel shows the adatom-hydrogen bond as well as the Si-Si vertical bond below the adatom (indicated by a filled arrow) which has higher energy than in the intrinsic surface. The fifth panel and the sixth panel show no change. It is noticeable that the hydrogen saturation removes the bond between the adatom and the atom right below it as indicated by an empty arrow in the seventh panel. The eighth and ninth panels show the Si-H bond states.

Fig. 3-8 shows the charge density cross section spectra in the presence of the hydrogen atom on the left rest atom as indicated in the top panel. The change of the spectra from those of the intrinsic surface show that the rest atom dangling bond state is lower in energy by 1.5 eV due to the formation of a Si-H bond. On the other hand, the dangling bond state of the other rest atom does not chage, and the dangling bond state of the corner hole atom is lowered in energy as shown in the second and the third panels. The fourth and the fifth panels show no change. The sixth through the ninth panels show the Si-H bond on the rest atom. All the remaining properties of the charge density cross section spectra are identical to those of the intrinsic surface.

Fig. 3-9 shows the charge density cross section spectra in the presence of the hydrogen atom on the corner hole, as indicated in the top panel. The only significant changes of the spectra from those of Fig. 3-6 are the lower energy of the corner hole dangling bond state due to the formation of a Si-H bond, from the range [0.0 eV, -0.5 eV] to the range [-3.0 eV, -4.0 eV] as shown in the eighth and ninth panels. Except

for the corner dangling bond state, all the rest of the charge density distributions remain unchanged from those of the intrinsic surface.

The changes of the surface electronic structure induced by hydrogen adsorption have strong *non-local* characteristics. Figs. 3-7 and 3-8 show that the presence of hydrogen on the unfaulted side changes the dangling bond state energy of the rest atom on the faulted side. These non-local interactions between the surface dangling bonds are induced by *charge transfer* between them. On the intrinsic $(7 \times 7)$ surface the adatom dangling bonds and the rest atom dangling bonds are partially filled, whereas the corner hole dangling bond is completely filled. Since the hydrogen atom is strongly electronegative, when the hydrogen is interacting with a partially filled dangling bond it attracts extra electron charge density to fill the interacting silicon dangling bond. This extra charge comes from the rest of the dangling bonds since they are more chemically reactive and more likely to donate charge than saturated bonds.

The hydrogen on the adatom attracts charge from both rest atom and corner hole dangling bonds so that these states become less filled, and consequently are changed in energy (A small increase of the Fermi level by 0.03 eV indicates the small charge transfer from the rest of the adatom dangling bonds.). Furthermore, the bonding charge between the adatom and the atom right below it is also transferred to the silicon-hydrogen bond as noted in the seventh panel of Fig. 3-7. The hydrogen on the rest atom also attracts charge from the other rest atom dangling bonds and the corner hole dangling bond so that those states become less filled, and their energies are also raised similar to the case of the hydrogen on the adatom. However, the hydrogen on the corner hole atom does not induce a non-local charge transfer from other dangling bonds. The corner hole dangling bond is already completely filled by two electrons, and the hydrogen adsorption actually introduces an excess electron so that there are three electrons to fill the Si-H bond. Two of these electrons form the corner hole Si-H bond, and the remaining electron is placed at the Fermi level as indicated by an upward shift of the Fermi level by 0.1 eV. This extra electron is distributed over 12 adatom dangling bonds and increases the adatom dangling bond fillings by about

8%. This small increase of dangling bond charge density, which is already quite small as shown in the second panels of Figs. 3-6, 3-7, 3-8, and 3-9, is difficult to discern in the gray scale of these plots. Nevertheless, a careful comparison of the second panels of Figs. 3-6 and 3-9 shows what appears to be a slight increase of the charge on the third dangling bond from the left.

The differences of the adsorption energies for H on adatom, rest atom, and corner hole respectively reflect energy costs of the non-local charge transfer among the dangling bonds, rather than differences in the Si-H bonding strength at different sites. A charge transfer leads to an increase of the energies of the involved dangling bonds so that a larger charge transfer corresponds to a larger energy cost. The adsorption energy on the adatom is smallest because it involves more charge transfer from the other dangling bonds and the bond between the adatom and the atom right below it. The adsorption energy on the corner hole atom is largest because no charge transfer cost is involved. One can estimate the energy cost of charge transfer for hydrogen on the adatom and on the rest atom as 0.6 eV and 0.3 eV from the differences of the adsorption energies. It is also noticeable that the adatom and rest atom adsorption energies are smaller than the adsorption energy of 1ML of hydrogen on the Si(111)-(1 $\times$ 1) surface (3.5 eV). Since the dangling bonds on this surface are uniformly saturated, no charge transfer is required to satisfy the Si-H covalent bonding.

## 3.5 Local Density of States

In order to make contact with experimental measurements, the local densities of states (LDOS) on the adatom, the rest atom, and the corner hole are calculated and shown in Figs. 3-10, 3-11, and 3-12. Fig. 3-10 shows that the LDOS on the adatom is strongly changed only when the hydrogen atom is adsorbed on the adatom, but the effect of the hydrogen atom on the rest atom and the corner hole does not significantly change the position of the peaks in the LDOS. The LDOS peak near the Fermi level indicates that the Si-H bond formation lowers the adatom dangling bond energy by about 1 eV [48] (Note that this energy shift should not be interpreted as the Si-H bonding

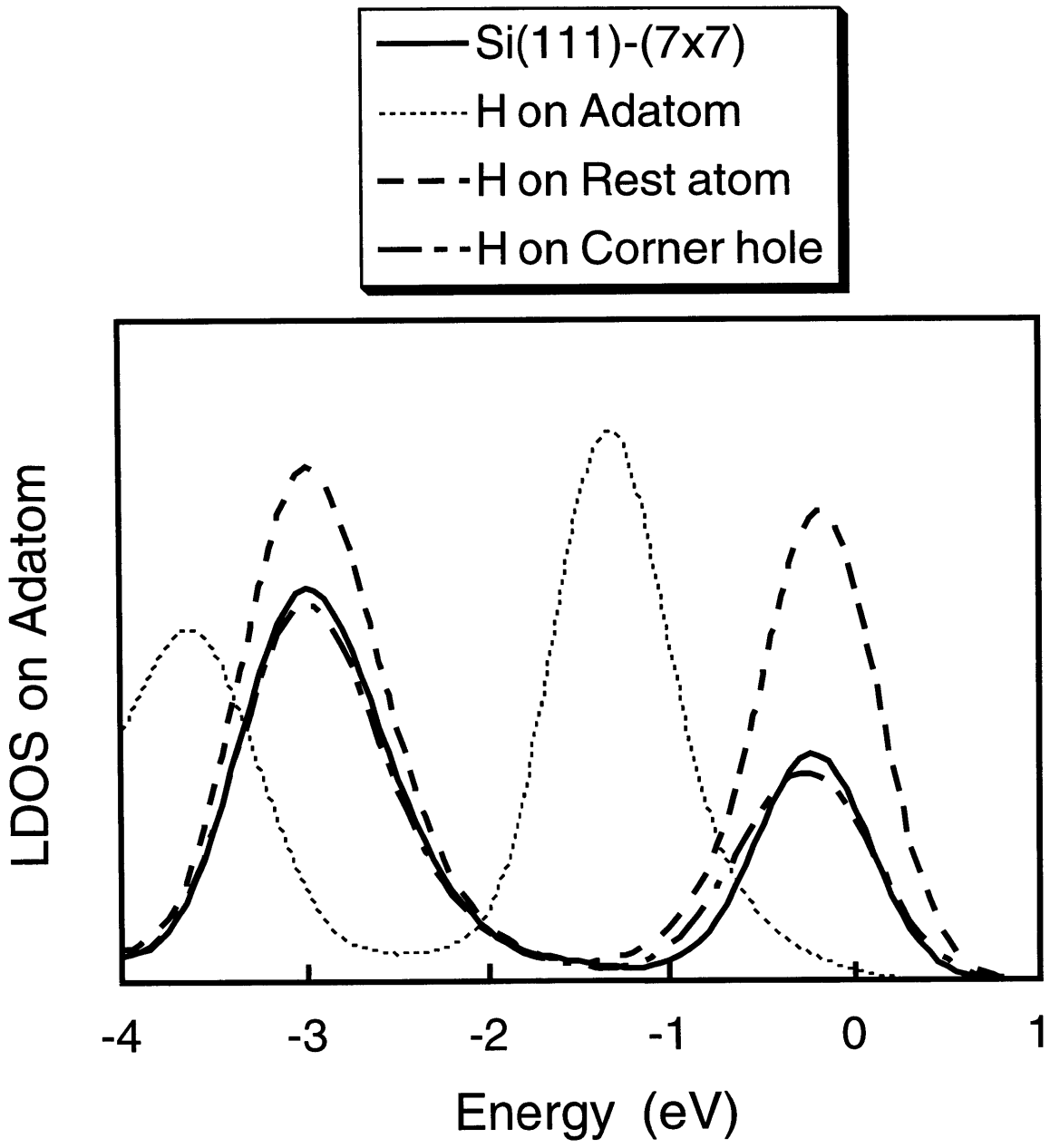


Figure 3-10: Plot of the local density of states on the adatom.

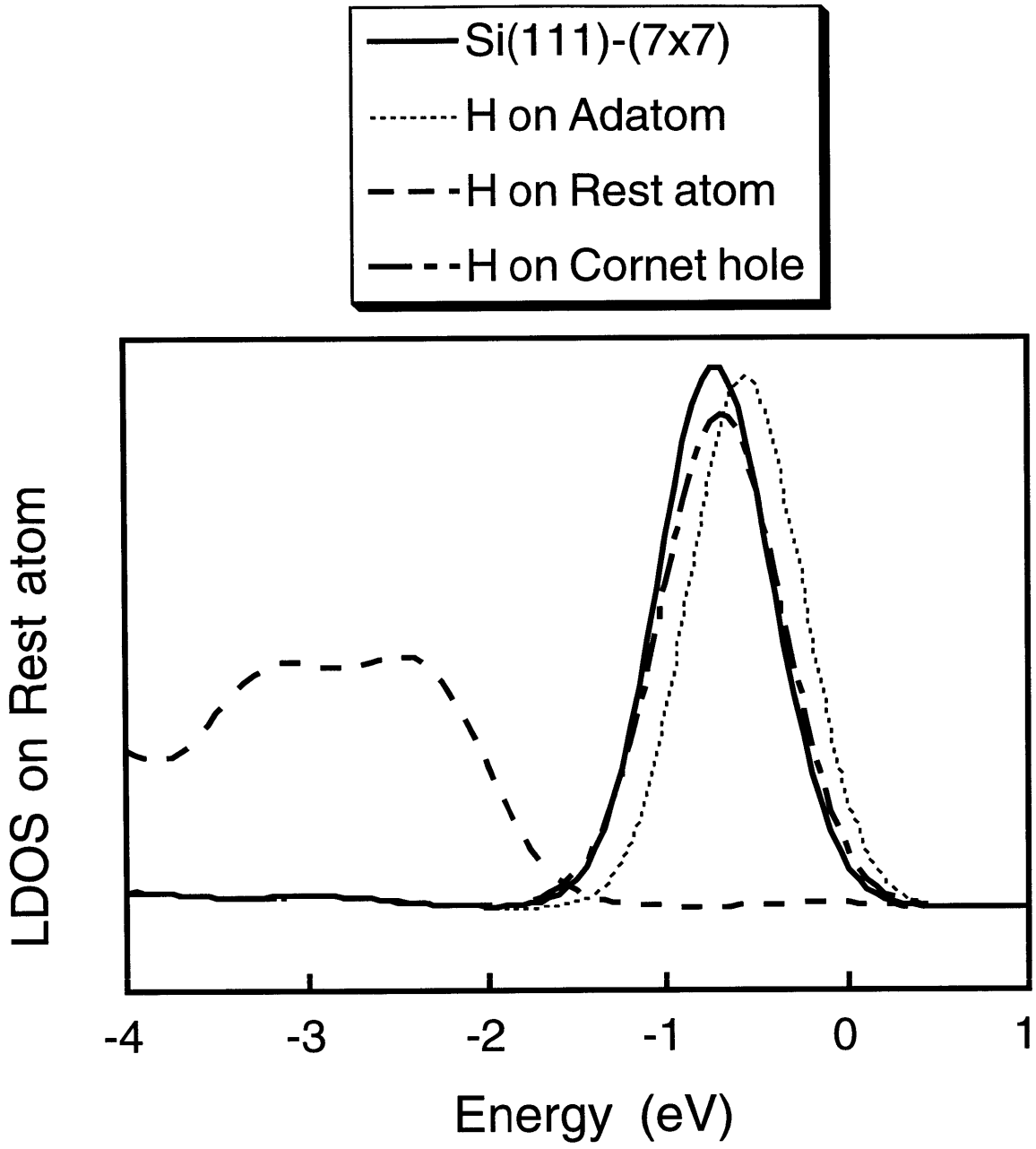


Figure 3-11: Plot of the local density of states on the rest atom.

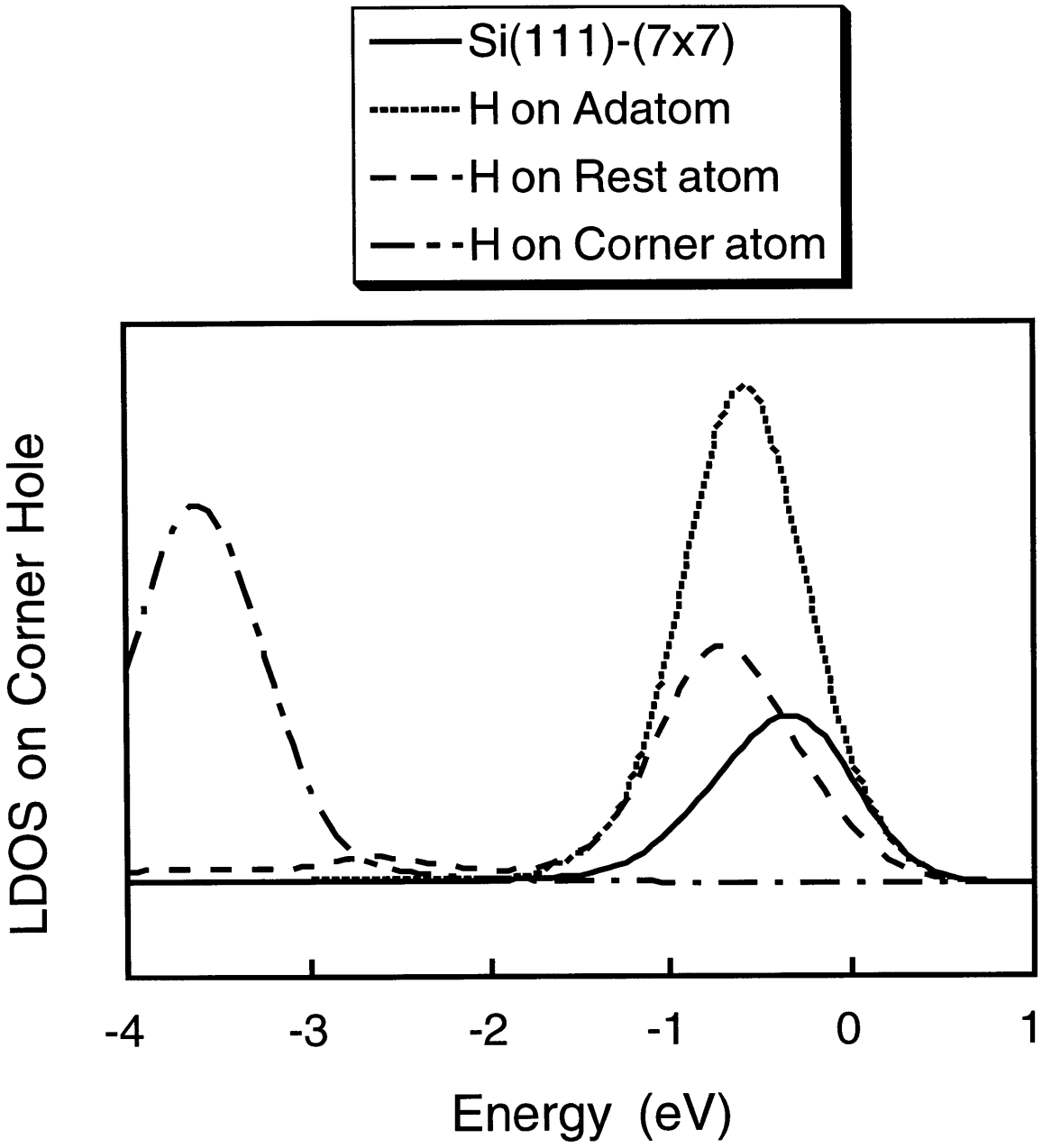


Figure 3-12: Plot of the local density of states on the corner hole atom.

strength because this is showing only a part of the Si-H states distributed over 10 eV energy range as discussed in Ref. [48]). It is noticeable that there are two LDOS peaks that originate from the adatom dangling bond states, separated in energy by about 3 eV. These correspond to two peaks in the differential conductivity observed in scanning tunneling spectroscopy (STS) measurement at the adatom position [40].

Fig. 3-11 shows the LDOS on the rest atom. The Si-H bond formation lowers the rest atom dangling bond energy by about 2 eV so that no local states are in the energy range between -2.0 eV and 0.0 eV, in agreement with STS measurements [40]. When the hydrogen atom is adsorbed on the adatom, the LDOS peak moves higher in energy due to charge transfer from the rest atom dangling bond to the adatom dangling bond, but this change is too small to be detected in STS measurements. The effect on the LDOS of hydrogen adsorption at the corner hole site is negligible.

However, Fig. 3-12 shows significant changes of the LDOS peak position due to hydrogen adsorption. The Si-H bond formation lowers the energy of the corner hole dangling bond by about 2 eV, while the non-local charge transfer from the corner hole dangling bond to the Si-H bond on the adatom or the rest atom moves the LDOS peak from the Fermi level. Consequently, the LDOS on the corner hole shows the results of the non-local charge transfer. Based on this we expect that the corner hole sites on the $(7 \times 7)$ reconstruction will exhibit significant changes in chemical reactivity induced by the non-local charge transfer due to adsorption.

To gauge the detectability of this effect by the STS measurements at the corner hole site, the LDOS on the corner hole is compared to the LDOS on the adatom. Since the depth of the corner hole in the STM measurement is 2 Å, the LDOS on the corner hole is calculated at a vertical position 2 Å lower than that of the LDOS on the adatom. This comparison shows that the intensities of the corner hole LDOS is an order magnitude smaller than the adatom LDOS, and for all practical purposes the corner hole LDOS is not detectable in STS measurements. This finding is consistent with the observations of no specific peak spectra on the corner hole site in the STS experiments [49]. Consequently, the first-principles spectral analysis of the electronic structure provides information of chemical reactivities on the surface sites (*i.e.*, corner

holes) which are not detectable by a scanning tip in STS measurements.

## 3.6 Conclusions

The calculated hydrogen adsorption energies are consistent with the chemical reactivity analysis based on the local charge densities of the surface dangling bonds. The adsorption induced relaxation of the local geometry is negligibly small, and the variation of the Si-H bond length is also small. However, there is significant charge transfer among dangling bonds induced by hydrogen adsorption, and the charge transfer leads to non-local changes of the surface chemical reactivity.

# Chapter 4

# The Nature of a Wet Electron

A comprehensive state-of-the-art *ab initio* study is performed on the wet electron – an electron interacting with a small cluster of water molecules – in the water hexamer system. Predictions include two previously unknown distinctive geometries which bind the excess electron as internal and external states, photoemission ionization energies in agreement with experiment, identification of generic electrophilic sites involving dangling hydrogen atoms, and the tendency of all hydrogen atoms to be saturated in hydrogen-bonding or in interaction with the excess electron. An emerging insight is the capability of electrophilic sites to be actuators of electron transport pathways in biomolecular systems.

## 4.1 Introduction

Studies of electrons bound to molecular systems are important for the ultimate understanding of phenomena associated with electron transfer, radical chemical reactions, and polarons [50, 51, 52, 53, 54, 55, 56, 57]. One classic and fundamental prototypical system involves the interactions of an electron with water molecules. Solvated electrons (i.e. electrons immersed in liquid water) are believed to be trapped in a cavity space bounded by six water molecules [51]. Such electrons have been the subject of intensive investigation since their transient optical spectra were first identified [52]. From spin echo modulation analyses, Kevan [51] inferred that an electron is hydrated

by six water molecules in an octahedral configuration with one O-H bond in each water molecule oriented toward the electron. The existence of such a configuration suggests that it is also possible for an excess electron to be bound to an *isolated* water cluster. Such an electron is often referred to as a "wet" electron.

Since an electron is not bound to a single water molecule, the localization of a wet electron is believed to depend on cluster size. From quantum path-integral calculation using model interaction potentials, Barnett *et al.* [53] suggested that anion water clusters, $e + (H_2O)_n$, with $n = 8 - 64$, can exist with a novel surface state of an excess electron. In recent mass spectrometer experiments various gas-phase water cluster anions were observed [5-6], but for the case of $n < 10$, clusters with only $n = 2, 6$, and7 were identified with certainty. Of particular interest is the case of $n = 6$ (water hexamer anion), since the solvated electron is also coordinated to six water molecules. Except for photoemission ionization energies (IE's), little is known experimentally about the water hexamer anion. Moreover, because of the complexities of dealing with a fully quantum mechanical problem, *ab initio* theoretical investigations of this system have been limited [56, 57]. Indeed, to our knowledge, an optimized geometry and electronic structure of the water hexamer anion, as well as the nature of the interaction forces in the system, are first reported.

## 4.2 Methods

Here, we present the first extensive ab initio theoretical investigation of an excess electron interacting with the electrons and nuclei of six water molecules. To ensure accuracy and reliability we employ two *ab initio* computational methods which are at the state-of-the-art, respectively, in quantum chemistry and condensed matter physics. Specifically, as a quantum chemical approach, the post Hartree-Fock theory including electron correlation based on the Møller-Plesset second order perturbation theory (MP2) is used with a Gaussian-type basis set including diffuse basis functions (6-311++G** basis set). A. T. Pudzianowski [58] has recently shown that use of MP2/G-311++G** can provide a good description of the energetics and structures

of anionic molecular systems. The calculations were performed using a Gaussian 92 suite [59] (written by M.J. Frisch *et al.* Gaussian Inc., Pittsburgh, 1992). As a condensed matter physics approach, density functional theory (DFT) is employed with separable pseudopotentials [30] and a gradient-corrected exchange potential [8] to the local part of the density functional [6] using a plane wave basis set (The benefit of using plane wave basis is that it provides an unbiased description of the electron density in any region of the cluster) in an iterative minimization relaxation scheme [36]. The DFT calculations were performed using a molecular dynamics-conjugate gradient program [36, 45]. A plane wave cutoff of 30 Ry was used corresponding to about 63000 plane waves in a supercell of $[15\text{Å}]^3$. In this study the structures were first fully optimized with MP2/6-311++G** calculations. Then, the electronic structure was studied using the DFT calculations with monomerical geometries relaxed. The results of both methods lead to a consistent and novel picture of a wet electron with possible implications for novel through-space (as opposed to through-bond) pathways in electron transport.

## 4.3 Results

We begin by placing six water molecules in Kevan's octahedral geometry [51] shown in the top panel of Fig. 4-1 with an excess electron. Although this geometry is strictly for a solvated electron, it is a reasonable starting point for the hexamer anion as well. Allowing all the atoms and electrons to relax, we obtain the triangular-rings structure shown in the middle panel of Fig. 4-1. In this geometry, the distances from the cluster center (Ct) to H, H′, and O atoms are 2.85, 3.34, and 3.47 Å, respectively. Here, H and H′ denote the H atoms at the shorter and longer distances from Ct, respectively. This relaxed structure is different from the octahedral geometry in a significant way: the OH bonds no longer point directly toward the center of the cluster. The relaxation allows hydrogen-bonding between adjacent molecules by forming two triangular rings. This structure, however, is only a local minimum energy geometry. We have discovered that a lower energy resonance geometry (by 0.26 eV in MP2 and

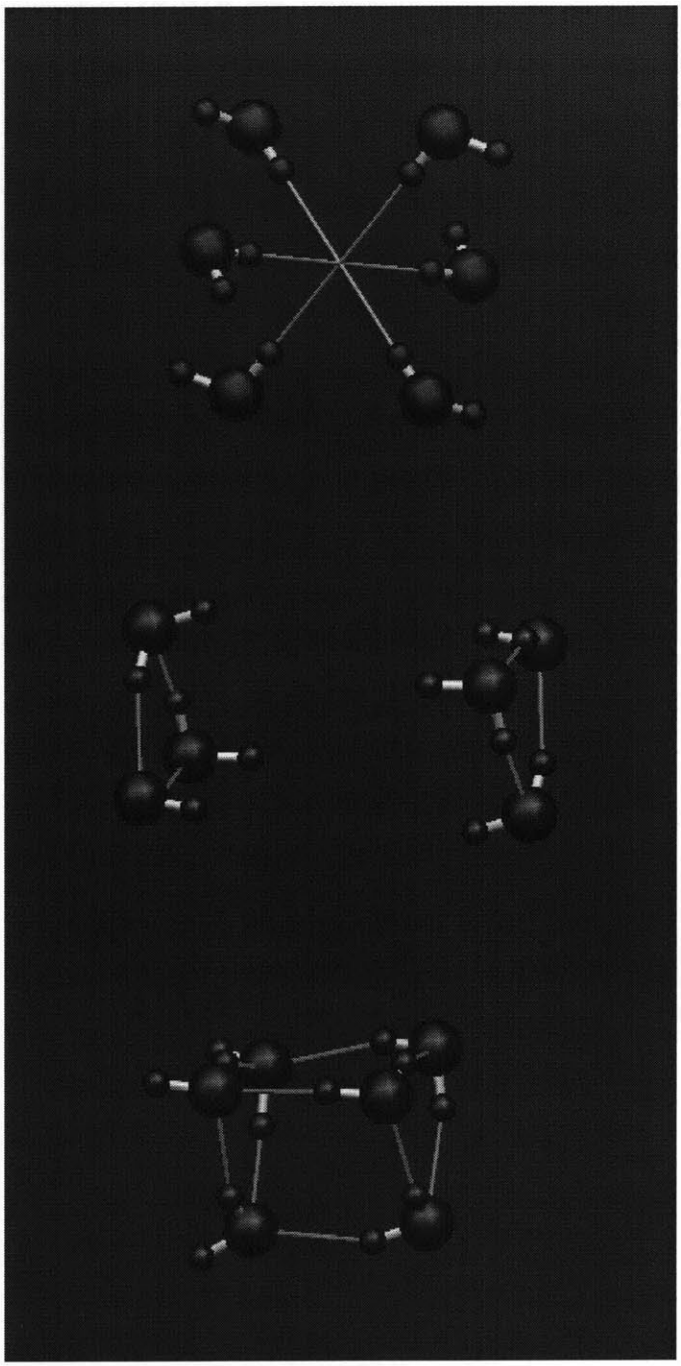

Figure 4-1: Possible hexamer anion geometries: octahedral structure of a solvated electron from Ref. [51] (top), triangular-rings structure (middle), and prism structure (bottom). Oxygen and hydrogen atoms are indicated respectively, as large and small black spheres. The lines in middle and bottom figures indicate hydrogen-bonding.

0.35 eV in DFT) is the prism structure shown in the bottom panel of Fig.4-1. For this geometry, the shortest interoxygen distances are 2.92 Å(upper triangle), 2.86 Å(lower triangle), and 2.92 Å(between triangles). The MP2/6-311++G** energy is -457.86088 hartrees.

The nature of the excess electron is illustrated in Fig. 4-2. Here are plotted valence electron charge distributions of the highest occupied molecular orbitals (HOMO) for the triangular-rings and prism structures, respectively. In the triangular-rings structure the electron is well localized inside the cluster and acts to bridge the two rings. Within a sphere encompassing the six oxygen atoms we find 57% of the excess electron. This electron has somewhat of an s orbital-like distribution which is similar in spirit to the predictions made in calculations of the condensed phase [60] and of the hexamer at Kevan's geometry [57]. It differs in that the electron density is described by six maxima distributed among very specific H atoms. These are 'dangling' H atoms that are not involved in hydrogen-bonding. A similar effect is manifested in the electron density distribution for the prism structure shown in the bottom panel of Fig. 4-2. The dangling H atoms act as electrophilic sites attracting the excess electron. This is certainly a reasonable result since H atoms involved in hydrogen-bonding are loosely speaking already 'saturated' electrophilic sites. All of the H atoms in an anionic cluster, therefore, appear to be involved in either hydrogen-bonding or in an interaction with the excess electron.

In comparison, in Fig. 4-3, we show electron charge distribution of the lowest unoccupied molecular orbitals (LUMO) for the same two structures. LUMO states have somewhat of a p-orbital-like distribution. There are two other p-orbital-like LUMOs for each structure which are not shown in the figure. The three p-orbital-like LUMOs for each structure do not have exactly the same energies. These result are also consistent with the condense phase study of Ref. [60], in which the transition from the ground state to three localized p-orbital-like states dominate the broad asymmetric spectrum with excited electrons. Even though, in anionic hexamers, LUMO states are not bound but are at resonant states (LUMO energies are about 0.1 hartrees), we can see that the dangling H atoms again act as electrophilic sites attracting the

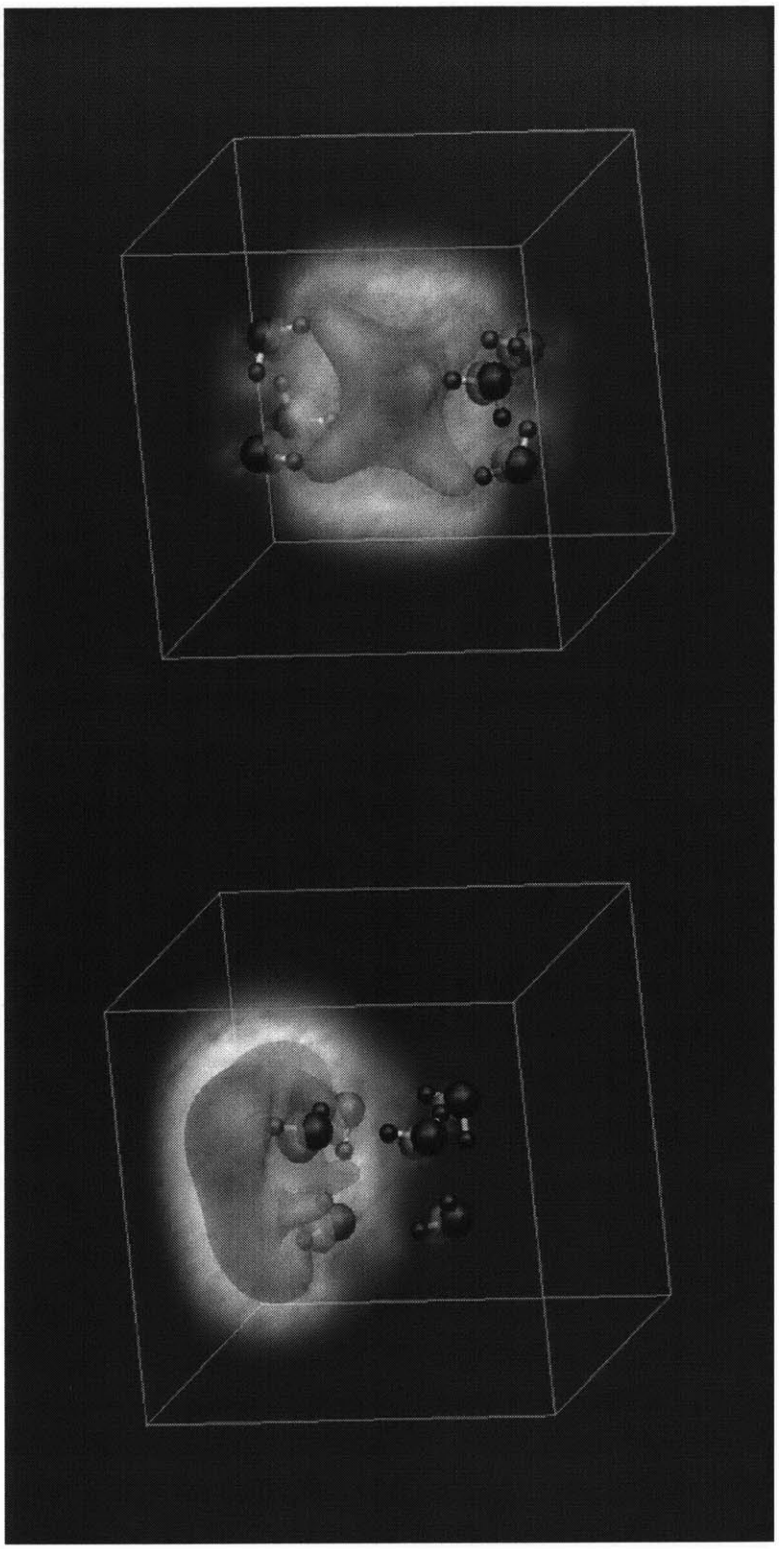

Figure 4-2: HOMO electron density distributions for the triangular-rings structure (top) and prism structure (bottom). Low to high densities are represented by bright to dark clouds.

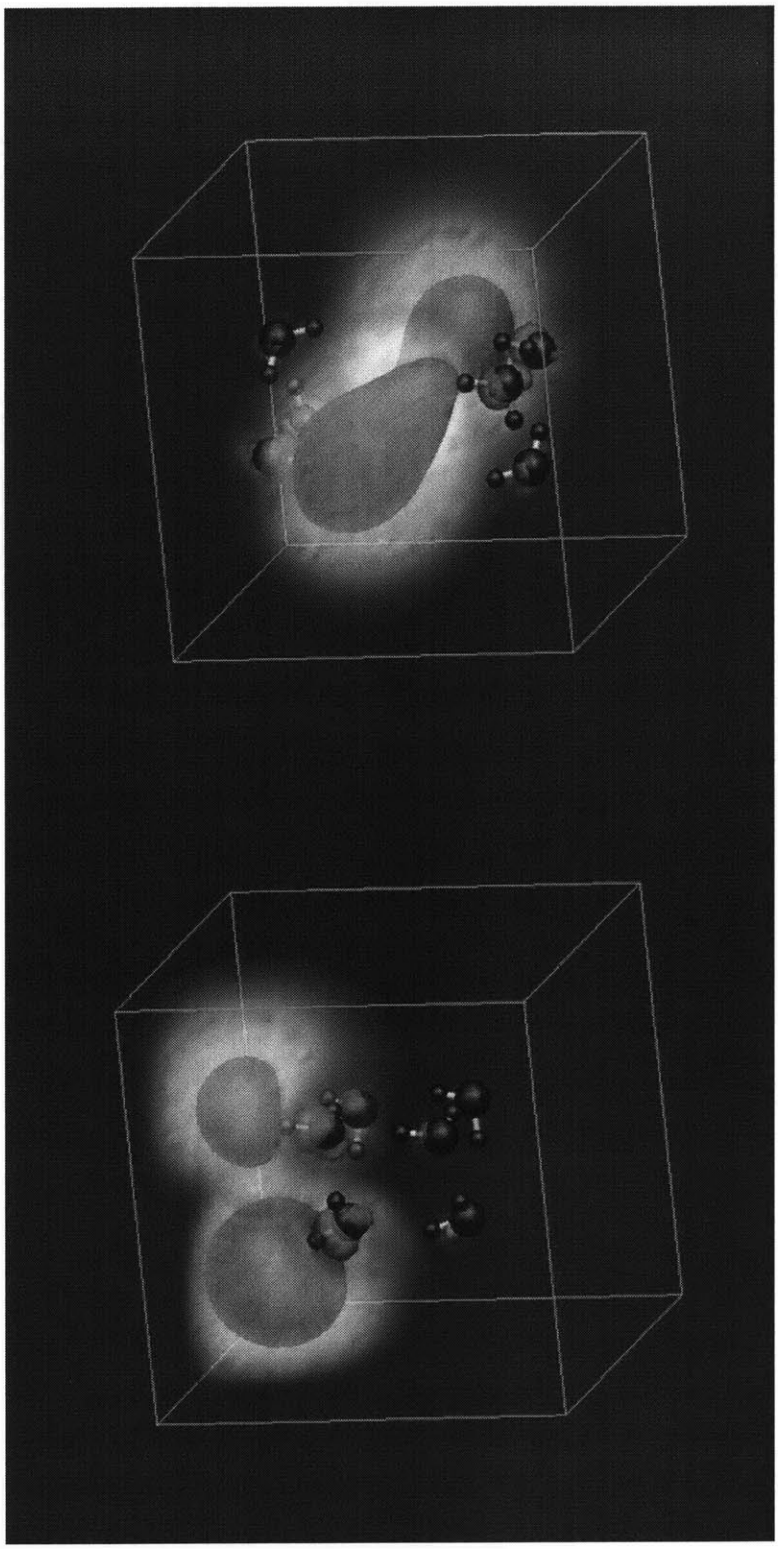

Figure 4-3: LUMO electron density distributions for the triangular-rings structure (top) and prism structure (bottom). Same convention as in Fig. 4-2.

excess electron just as in the case of the ground states.

As further evidence of these effects, we show in Fig. 4-4 the results for two other cluster geometries. These geometries were obtained from the nearly isoenergetic ground state structures of the neutral hexamer [61]. One of these (top panel) is a prism-derivative structure (PD), and the other (bottom panel) is a cyclic structure. For PD structure, the neighboring inter-oxygen distances are 2.80-2.89 Å(upper triangle), 2.91-2.98 Å(lower triangle), and 2.92 Å(between two triangles). For cyclic structure, the distances from Ct to H, H′, and O atoms are 2.26, 2.72, and 2.59 Å, respectively. Both clusters are characterized by excess electron HOMO states that are resonances. They are stable in their neutral configurations. They both clearly show that the excess electron even in resonant states, is attracted to the dangling H atoms. Furthermore, the surface states observed in the medium-sized water clusters by Barnett *et al.* [53] are related to the electrophilic cluster sites, with the dangling H atom sites acting as actuators of these surface states. Kevan's structure of the electron bound in liquid water also demonstrates that the dangling H atoms are the actuators of the internal states.

Of all the geometries we have studied, we find that only the triangular-rings and prism structures bind an excess electron. Both the triangular-rings and prism structures are metastable with the excess electron. At the level of the MP2/6-311++G** theory, the anionic prism structure is higher ( 0.5 eV) in energy than the neutral cyclic hexamer with the electron at infinity. The significant difference between the electron distribution of the triangular-rings and prism structures is reflected in a significant difference in our predicted IE's, which are 0.5 and 0.1 eV, respectively. Here the photoemission IE's (or vertical electron detachment energies) have been calculated by subtracting the total energy of the anionic species from that of the neutral species at the optimized geometry of the anionic structure. The agreement with the experimental IE's, which are 0.5 eV and 0.2 eV [55], is notable. This indicates that the observed IE's arise from two separate classes of cluster geometries rather than two states of the same cluster. However, the experimental photoemission signal is found to be much stronger at 0.5 eV than at 0.2 eV. This might appear to be evidence against the

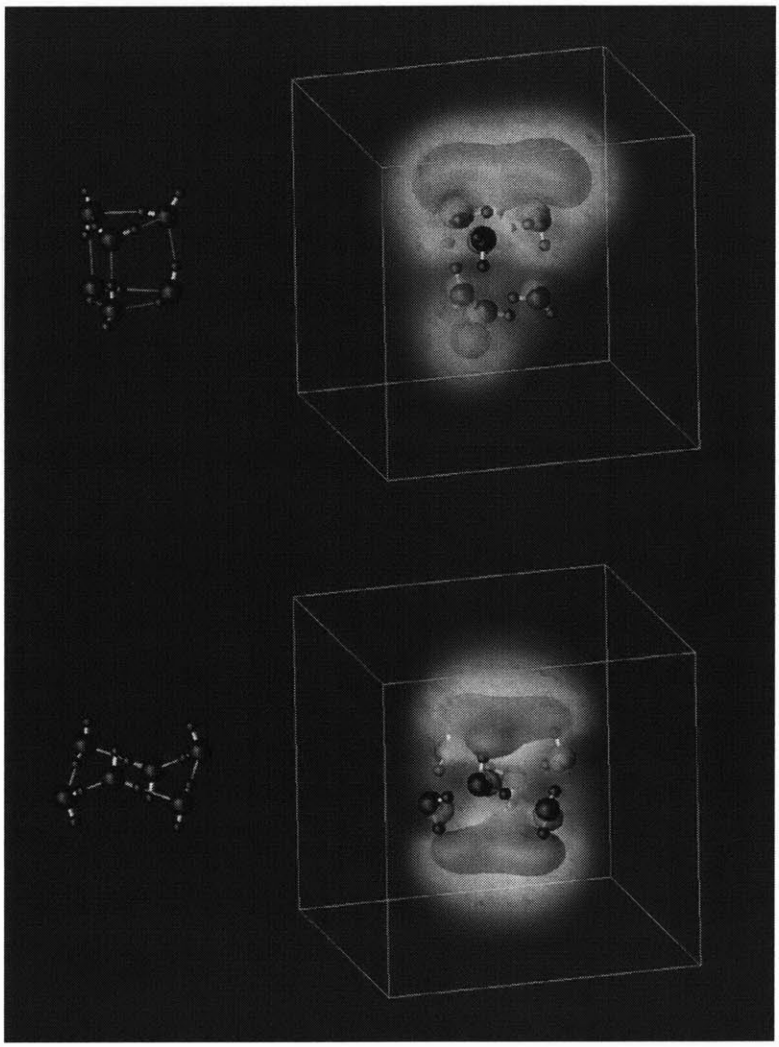

Figure 4-4: HOMO electron density distributions for the prism-derivative structure (top) and cyclic structure (bottom) in resonance states. Same convention as in Fig.4-2.

prism geometry having a ground state energy lower than that of the triangular-rings geometry. But a simple analysis of the appropriate Fourier components of the excess-electron wavefunctions shows that the triangular-rings HOMO-state has a much larger photoemission cross section than the prism HOMO-state (by ~103), which leads to consistency with the photoemission spectrum.

Our overall results can be understood using a simple heuristic based on the energetics of hydrogen bond formation and the nature of the excess electron-hydrogen ($e \cdots$ H) interactions. The $e \cdots$ H interaction is strongly cooperative in that the electron density favors clustered dangling H atoms. This is reflected in the energy difference between the prism and prism-derivative structures. The $e \cdots$ H interaction induces the prism structure, which is less stable (0.2 eV) in the neutral state than the prism-derivative structure, to become more stable (0.1 eV) in the anionic state. It also induces the triangular-rings structure, which is highly unstable in the neutral state, to become stable in the anionic state. Thus the $e \cdots$ H interaction emerges as an important force, comparable to the hydrogen-bonding interaction. However, since the energies increase in going from prism to triangular-rings to Kevans structure, the $e \cdots$ H interaction is weaker than the hydrogen-bonding. Since all H atoms in the anionic clusters are involved in either hydrogen-bonding or $e \cdots$ H interactions, this saturation accounts for the isoenergetic nature of the anionic clusters. Moreover, the competition between the interactions generates more diverse conformers than in the neutral states. As a consequence, deionization of anionic clusters could be used to facilitate the formation of novel neutral conformers that are not easily accessible. The case of the prism structure is such an example.

## 4.4 Conclusion

Finally, an interesting insight emerging from this ab initio study is related to the generic electrophilic nature of the dangling H atoms. This nature should prevail even in more complex molecular environments. It is well known that water molecules can be embedded or attached to biomolecular systems. Conceptually, dangling H atoms

on strings or networks of such water molecules would allow an electron to hop between them and thereby actuate a pathway for electron transport. An analogy can be found with cation pathways in transmembrane channels, where oxygen atoms on the inside wall of the transmembrane play an important role in guiding cations through the channels [62]. As an example, in azurine dimers from pseudomonas aeruginosa [63], two water molecules bridging azurin monomers, have been identified as being involved in the electron transfer between the Cu(I) and Cu(II) redox centers in the respective monomers. Although the conformation of these water molecules is not known, in this system it is reasonable to expect one or two dangling H atoms in the cluster. The results of our work would then suggest that through-space electron transport between monomers could then take place through these electrophilic sites. Of course, we have not included the effects of dynamics or solvents which are beyond the scope of this work. Nevertheless, the generic electrophilic nature of the dangling H atoms should be fairly robust, and it would be exciting if it proves possible to harness this property to effect novel through-space pathways for electron transport in addition to the traditional through-bond pathways.

# Chapter 5

# Excess Electron Transport in Water

The microscopic transport processes of an excess electron in bulk water are studied using *ab initio* molecular dynamics calculations. In contrast to the typical cavity obtained with solvated anions, the electron cavity structure is found to be much more variable, with water molecules easily exchanging at the surface of the cavity. The microscopic mechanism of electron transport involves a novel sequence of opportunistic electron redistributions driven by a positive feedback between thermal fluctuations and the attraction of the electron to hydrogen atoms that are not saturated in hydrogen bonding.

## 5.1 Introduction

Unraveling the microscopic details of the solvation dynamics of an excess electron in bulk water has been a problem of ongoing interest for the past 20 years [51, 64, 65, 66, 67, 68, 69, 70, 71, 72, 73, 74]. The presence of strong hydrogen bonding interactions in water induces complex structural rearrangements of water molecules in order to accommodate an excess electron. From spin echo modulation analyses, Kevan has inferred that the excess electron is hydrated by six water molecules in an octahedral cavity configuration with one OH bond of each water molecule oriented toward the

electron at the center [51]. Recent theoretical studies of an excess electron interacting with classical water molecules have demonstrated that an electron injected into bulk water induces a structural rearrangement of nearby water molecules to form a cavity-like structure within 1 psec [68, 69]. Because the solvation energy of an excess electron is large (about 2-3eV), it would appear that the electron water molecule complex might be similar to that of solvated anions. But its diffusion constant is found to be 2-3 times larger than those of solvated anions with similar cavities. Moreover, the lighter mass of a classical electron is not sufficient to account for this [70]. Several mechanisms [71, 72, 73, 74] to address this rapid transport have been proposed and it is now believed that polaronic behavior plays a central role in the transport of an excess electron in water [73, 74]. However, the details of the microscopic transport process have yet to be identified. In a recent theoretical study of the anionic water hexamer, it was predicted [75, 76] and subsequently observed [77], that the excess electron mainly interacts with the *dangling* hydrogen atoms, i.e., the hydrogen atoms which are not directly involved in hydrogen bonding. This suggests that the interactions between an excess electron and dangling hydrogen atoms should also influence, and possibly dominate, the dynamical transport precesses of this excess electron in liquid water.

In this work, we report the results of an extensive *ab initio* molecular dynamics study of an excess electron in bulk water. The focus of this investigation is to elucidate the stability of the cavity structure and the microscopic details of transport of the excess electron. Because of the difference in required-accuracy and time-scale of these two processes, we perform *ab initio* calculations using both ionic pseudopotentials and molecular pseudopotentials in a complementary manner. Specifically, two sets of calculations are undertaken with well-defined goals. To study cavity stability and relaxation, which requires longer simulation time but not a detailed description of the electron, all the water molecules are taken to be described by a molecular pseudopotential. To study the detailed, very short time scale processes involved in electron transport, water molecules in the immediate vicinity of the electron are taken to be the appropriate number of hydrogen and oxygen atoms, each described in terms of an ionic pseudopotential. The rest of the water molecules are again described in

terms of molecular potentials. As we discuss in what follows, both sets of calculations provide a consistent picture of the excess electron that elucidates the *dynamical stability* of the cavity structure and leads to a deeper understanding of the microscopic electron transport process.

## 5.2 Methodology

### 5.2.1 Stability of Cavity Structure Calculation

The stability and relaxation of the cavity structure of the excess electron are investigated using a model system of 112 water molecules plus one electron in a super-cell of dimension $[15\text{Å}]^3$. For this case, the interactions of the excess electron with the water molecules is described completely in terms of molecular pseudopotentials. Our pseudopotentials are similar in spirit to other molecular pseudopotentials [73, 74] and have the following form

$$\begin{aligned} V(\vec{r}) &= V_h(\mid \vec{r} - \vec{R}_{h1} \mid) + V_h(\mid \vec{r} - \vec{R}_{h2} \mid) \\ &\quad + V_o(\mid \vec{r} - \vec{R}_o \mid) + \widetilde{V}_o(\mid \vec{r} - \vec{R}_o, \mid) \end{aligned} \tag{5.1}$$

where $\vec{R}_{h1}$, $\vec{R}_{h2}$ and $\vec{R}_o$ are the positions of the hydrogen and oxygen atoms of a water molecule respectively, and $V_h(r)$ and $V_o(r)$ are given by

$$\begin{aligned} V_h(r) &= (a_h + z_h e/r)\exp(-(r/r_h)^3) - z_h e/r, \\ V_o(r) &= -z_o e/r \end{aligned} \tag{5.2}$$

and represent coulomb interactions (truncated for the hydrogens) with partial charges assigned to atomic sites. In addition to the coulomb terms, $V(\vec{r})$ contains a polarization term

$$\begin{aligned} \widetilde{V}_o(r) &= (a_o + z_o e/r)\exp(-(r/r_o)^3) \\ &\quad + b_o \exp(-(\mid r - w_o \mid /\sigma)^3) \end{aligned}$$

| | | | | | | |
|---|---|---|---|---|---|---|
| Hydrogen | $z_h$ | $r_h$ (Å) | $a_h$ (hartree) | | | |
| | 0.46$e$ | 0.45 | -1.4 | | | |
| Oxygen | $z_o$ | $r_o$ (Å) | $w_o$ | $\sigma$ | $r_c$ | $r_{\rm pol}$ |
| | -0.92$e$ | 0.52 | 0.55 | 0.56 | 0.80 | 10.0 |
| | $a_o$ (hartree) | $b_o$ | $\alpha$ (hartree/Å$^4$) | | | |
| | -0.12 | 0.55 | 124.3 | | | |

Table 5.1: Parameter values for molecular pseudopotentials.

$$-\frac{1}{2}\alpha/(r^2+{r_c}^2)^2(1-\exp(-(r/r_c)^2))$$
$$\exp(-(r/r_{pol})^3) \tag{5.3}$$

where $\alpha$ is the average polarizability of water molecules. The first two terms in $\widetilde{V}_o$ are needed to control the $r = 0$ behavior of the potential. The various parameters are given in Table. 5.1 and are determined as follows. The parameters $z_h$ and $z_o$ are fit to the dipole moment of a neutral water molecule and the parameter $\alpha$ is obtained from experiment. All other parameters are obtained by fitting this form of $V(\vec{r})$ to *ab initio* density functional calculations of the wavefuction and energy associated with an excess electron in an isolated water molecule described by ionic pseudopotentials. These parameters are then tested successfully to predict the corresponding properties of a water *dimer*. In this case two dimer calculations are actually performed. In the first calculation, both water molecules are described in terms of ionic pseudopotentials. In the second calculation, one of the water molecules is described in terms of the molecular pseudopotential. We find that the molecular pseudopotential can accurately reproduce the excess electron distribution, not only for the static case, but also for the case of room temperature vibrational motions within 6%.

To describe the inter and intra molecular interactions between the water molecules

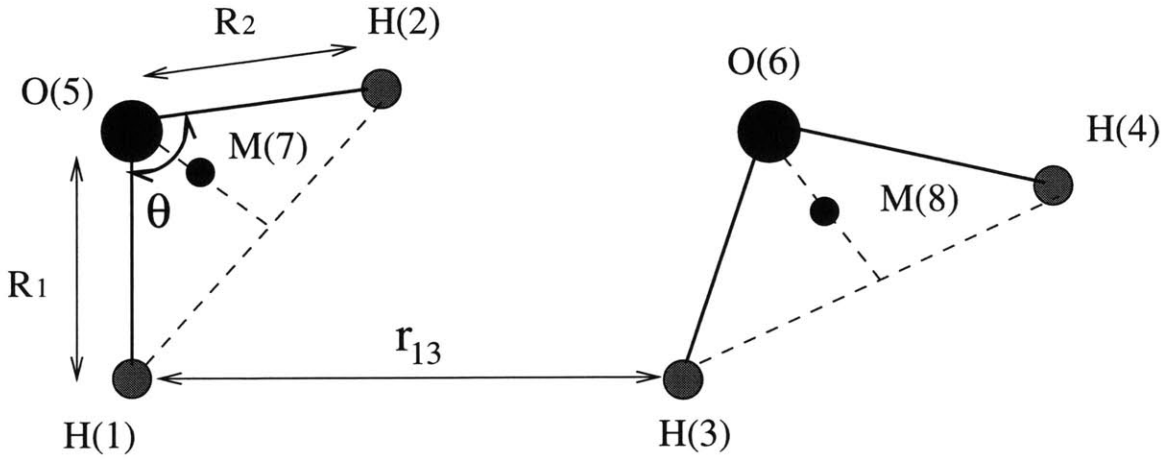


Figure 5-1: Geometric diagram identifying terms in the Lie-Clementi dynamical potentials used in this work. As an example, $r_{13}$ in Eq. (5.5) is the distance between H(1) and H(3). The lengths $R_1$, $R_2$ and the angle $\theta$ define two OH bond lengths and a H-O-H bond respectively. The corresponding equilibrium bond length $R_e$ and angle $\theta_e$ are 0.9576Å and 104.59° respectively. There is a charge q on each H atom and a charge -2q at each site M. M is chosen to lie on the bisection line connecting O and the center of the H-H line. The ratio of OM distance to the bisection line length is fixed to be 0.457.

we use the Lie-Clementi dynamical potentials [78] (see Fig. 5-1) of the form:

$$V(r_{\alpha\beta}, q_i) = V_{\text{inter}}(r_{\alpha\beta}; a_k) + V_{\text{intra}}(q_i) \tag{5.4}$$

The inter-molecular part is given by

$$\begin{aligned} V_{\text{inter}} &= q^2(1/r_{13} + 1/r_{14} + 1/r_{23} + 1/r_{24}) + 4q^2/r_{78} \\ &\quad -2q^2(1/r_{28} + 1/r_{18} + 1/r_{37} + 1/r_{47}) \\ &\quad +a_1 e^{-b_1 r_{56}} + a_2(e^{-b_2 r_{13}} \\ &\quad +e^{-b_2 r_{14}} + e^{-b_2 r_{23}} + e^{-b_2 r_{24}}) \\ &\quad +a_3(e^{-b_3 r_{16}} + e^{-b_3 r_{26}} + e^{-b_3 r_{35}} + e^{-b_3 r_{45}}) \\ &\quad -a_4(e^{-b_4 r_{16}} + e^{-b_4 r_{26}} + e^{-b_4 r_{35}} + e^{-b_4 r_{45}}) \end{aligned} \tag{5.5}$$

and contains both coulomb and repulsive core interactions. The intra-molecular potential is taken to be of following form,

$$\begin{aligned} V_{\text{intra}} &= \frac{1}{2} f_{RR}({\delta_1}^2 + {\delta_1}^2) + \frac{1}{2} f_{\theta\theta} {\delta_3}^2 \\ &\quad +f_{RR'}\delta_1\delta_2 + f_{R\theta}(\delta_1 + \delta_2)\delta_3 \\ &\quad +\frac{1}{R_e}[f_{RRR}({\delta_1}^3 + {\delta_2}^3) + f_{\theta\theta\theta}{\delta_3}^3 \\ &\quad +f_{RRR'}(\delta_1 + \delta_2)\delta_1\delta_2 \\ &\quad +f_{RR\theta}({\delta_1}^2 + {\delta_2}^2)\delta_3 + f_{RR'\theta}\delta_1\delta_2\delta_3 \\ &\quad +f_{R\theta\theta}(\delta_1 + \delta_2){\delta_3}^2] \\ &\quad +\frac{1}{{R_e}^2}[f_{RRRR}({\delta_1}^4 + {\delta_2}^4) + f_{\theta\theta\theta\theta}{\delta_3}^4 \\ &\quad +f_{RRRR'}({\delta_1}^2 + {\delta_2}^2)\delta_1\delta_2 \\ &\quad +f_{RRR'R'}{\delta_1}^2{\delta_2}^2 + f_{RRR\theta}({\delta_1}^3 + {\delta_2}^3)\delta_3 \\ &\quad +f_{RRR'\theta}(\delta_1 + \delta_2)\delta_1\delta_2\delta_3 \\ &\quad +f_{RR\theta\theta}({\delta_1}^2 + {\delta_2}^2){\delta_3}^2 + f_{RR'\theta\theta}\delta_1\delta_2{\delta_3}^2 \\ &\quad +f_{R\theta\theta\theta}(\delta_1 + \delta_2){\delta_3}^3, \end{aligned} \tag{5.6}$$

where $\delta_i = R_i - R_e$ $(i = 1, 2)$ and $\delta_3 = R_e(\theta - \theta_e)$ are changes in bond lengths $R_i$ and bond angle $\theta$ from their equilibrium values $R_e$ and $\theta_e$. Parameter values for both parts are given in Table. 5.2 and $r_{ij}$ is defined as in Fig. 5-1.

Electronic eigenstates are obtained using conjugate gradient methods in a plane wave basis with energy cutoff of 30 Ry [79] using the $\Gamma$ point for Brillouin zone integration. Ionic degrees of freedom are restricted to the Born-Oppenheimer surface by calculating Hellmann-Feynman forces within the accuracy of 0.05 $eV/$Å. The molecular trajectories are generated using the velocity Verlet algorithm with a time step of 0.5 fsec.

To investigate the rigidity of the cavity structure and to determine the influence of bulk water on known stable small anionic water clusters, we begin our simulation by restricting the water molecules to be in the Triangular Rings (TR) structure which is a stable state of the isolated charged water hexamer [75]. Initially, the system is equilibrated by placing a point charge electron [73] at the center of the TR hexamer structure surrounded by the remaining 106 water molecules. The hexamer anion structure is allowed to expand and shrink maintaining its relative configuration, while the surrounding 106 water molecules are equilibrated at room temperature for 3 psec. Subsequently, the molecular dynamics is followed for an additional 2 psec without imposing any constraints on the hexamer structure and with a quantum electron. As we shall see in section III.A, the TR structure rapidly decays into a cavity structure reminiscent of the Kevan geometry in about 200 fsec.

### 5.2.2 Electron Transport Mechanism Calculation

In this set of calculations, we examine in detail the very short time-scale evolution of the excess electron charge distribution. For this purpose we desire a more accurate description of the excess electron-water molecules interaction, and consequently we replace the six pseudo-molecules in the immediate vicinity of the excess electron by six water molecules made up of the appropriate number of hydrogen and oxygen atoms. The hydrogen and oxygen atoms are described in terms of optimized [27] ionic pseudopotentials of the separable form [30]. The electron-electron interactions are treated

| | | | | |
|---|---|---|---|---|
| $V_{\text{inter}}$ | | | | |
| | $a_1$ | $a_2$ | $a_3$ | $a_4$ |
| (kcal/mol) | 1088213.2 | 666.3373 | 1455.427 | 273.5954 |
| | $b_1$ | $b_2$ | $b_3$ | $b_4$ |
| ($\text{Å}^{-1}$) | 5.152712 | 2.760844 | 2.961895 | 2.233264 |
| | $q^2$ | | | |
| (kcal/molÅ) | 170.9389 | | | |
| $V_{\text{intra}}$ | | | | |
| | $f_{RR}$ | $f_{\theta\theta}$ | $f_{RR'}$ | $f_{R\theta}$ |
| ($10^5$dyn/cm) | 8.5120 | 0.7987 | -0.0967 | 0.2732 |
| | $f_{RRR}$ | $f_{\theta\theta\theta}$ | $f_{RRR'}$ | $f_{RR\theta}$ |
| | -9.497 | -0.1268 | -0.031 | -0.034 |
| | $f_{RR'\theta}$ | $f_{R\theta\theta}$ | $f_{RRRR}$ | $f_{\theta\theta\theta\theta}$ |
| | -0.512 | -0.1565 | 14.0 | -0.032 |
| | $f_{RRRR'}$ | $f_{RRR'R'}$ | $f_{RRR\theta}$ | $f_{RRR'\theta}$ |
| | -0.05 | 0.06 | -0.2 | 0.1 |
| | $f_{RR\theta\theta}$ | $f_{RR'\theta\theta}$ | $f_{R\theta\theta\theta}$ | |
| | -0.08 | 0.35 | 0.104 | |

Table 5.2: Parameter values for intra and inter molecular potentials. Values are taken from Ref. [78].

in density functional theory using the Perdew-Zunger local density approximation [6] and the Becke gradient correction to exchange [8]. There are three additional interactions that need to be taken into account. One is the coulomb interaction between ionic cores which we handle using the conventional Ewald method [13]. The second is the *repulsive* part of the interaction between the ionic cores and the pseudo-molecules which we simply take to be the non-coulomb part of Eq. (5.5). The third involves replacing $\widetilde{V}_o$ in Eq. (5.1) by $\mathcal{P}_v\widetilde{V}_o\mathcal{P}_v$, where $\mathcal{P}_v$ is a projection operator onto the excess electron states. This enables one to keep track and separate the polarization effects of the excess electron from the remaining electrons in the system whose contribution is already contained in $V_{\text{inter}}(r_{\alpha\beta}; a_k)$.

To perform the dynamical simulation, the initial configuration is taken to be the final configuration of the 2 psec run employing all pseudomolecular potentials as described earlier. Starting from the 2 psec positions, 6 water molecules located near the excess electron are replaced by the appropriate number of hydrogen and oxygen atoms and an *ab initio* molecular dynamics followed for 120 fsec without any structural constraints.

## 5.3 Results

### 5.3.1 Stability of Cavity Structure

Figure 5-2 shows three frames of the dynamics simulation at (a) 0 fsec, (b) 50 fsec, and (c) 2 psec after the 3 psec equilibration described in II.A. Brighter water molecules represent the original TR structure and the black lines represent the hydrogen bonds in the first shell. The TR structure is found to be unstable in bulk water and relaxes within 200 fsec to a structure that resembles a *Kevan-like* cavity structure, as described in section 5.1. It has an average of 6-7 hydrogen atoms pointing toward the excess electron within 3 Å from the center of the excess charge distribution. During the subsequent 1.8 psec of the dynamics simulation, the structure fluctuates significantly, but on the average a Kevan-like cavity is *stably* maintained. The fluctuations,

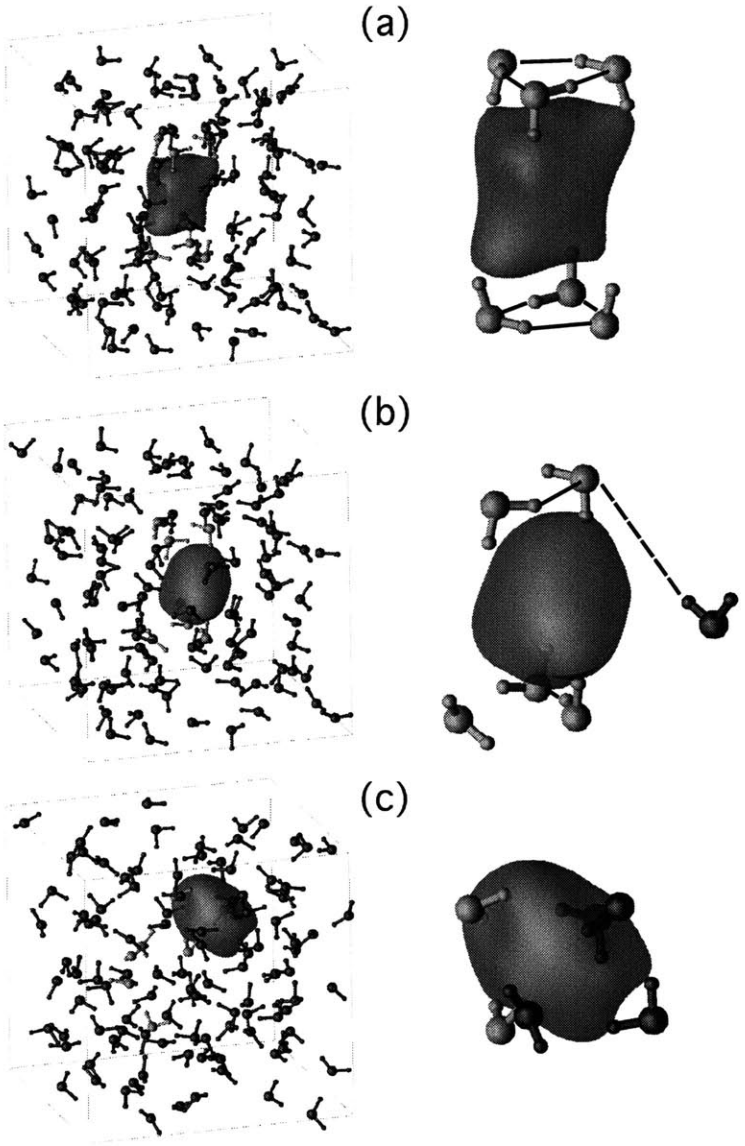


Figure 5-2: Room temperature dynamical simulation of 112 pseudo water molecules and an excess electron in a cubic super-cell at (a) 0 fsec, (b) 50 fsec, and (c) 2psec after a 3 psec effective equilibration. Right panels are enlargements of the first shell cavity structures. The excess electron charge distribution is shown as the isosurface and the six brighter water molecules identify the initial Triangular Rings hexamer structure. The solid lines represent hydrogen bondings among the water molecules that comprise each cavity. In (b) the dashed line indicates the formation of a weak hydrogen bond as a new water molecule becomes part of the first shell

viewed in the frame of reference of the electron, involve several water molecules leaving and entering the first shell of the cavity. Parts (a) and (b) show the configurations of water molecules and the excess electron charge distributions during the initial relaxation of the TR structure to a Kevan-like structure. After only 50 fsec, two water molecules have broken hydrogen bonds in the initial TR hexamer, and a new water molecule is moving into the first shell of the cavity. Fig. 5-2(c) illustrates a typical equilibrated Kevan-like structure. On the whole, the electron is distributed around the dangling hydrogen atoms of the water molecules in the first shell of the cavity.

To get a more quantitative measure of the relaxation process of the TR structure, oxygen velocity auto-correlation functions were calculated during the first 600 fsec portion of the run. Their fourier-transformed spectral densities are shown in Fig. 5-3. To gauge the role of the excess electron in the break-up of the initial TR structure, an additional molecular dynamics simulation was performed starting from a neutral TR structure without an excess electron. Figure 5-3 shows the low frequency spectral densities of the six oxygens in the initial TR hexamer with and without an excess electron. The spectral densities are calculated with two consecutive time intervals of 150 fsec shown as doted and dashed curves. The long time average equilibrium spectral density of bulk water is shown as a solid curve. For the neutral system (top panel), we note that the second interval spectral density is still quite different from the equilibrium spectral density. On the other hand, the spectral densities in the presence of an excess electron (bottom panel of Fig. 5-3) reveal a rapid relaxation to equilibrium.

This result may appear at first sight to be surprising since the TR structure is less stable without the excess electron than with it and therefore likely to begin breaking up sooner. The fact that we observe the opposite suggests that the difference between the two relaxation processes is basically caused by the excess electron's attraction to hydrogen atoms in process of breaking hydrogen bonds. Without an excess electron the relaxation of the TR structure proceeds through the breaking of hydrogen bonds in the hexamer (with a barrier of about 0.2 eV) and this makes the relaxation slow. However, in the presence of an excess electron, a broken hydrogen bond is immediately

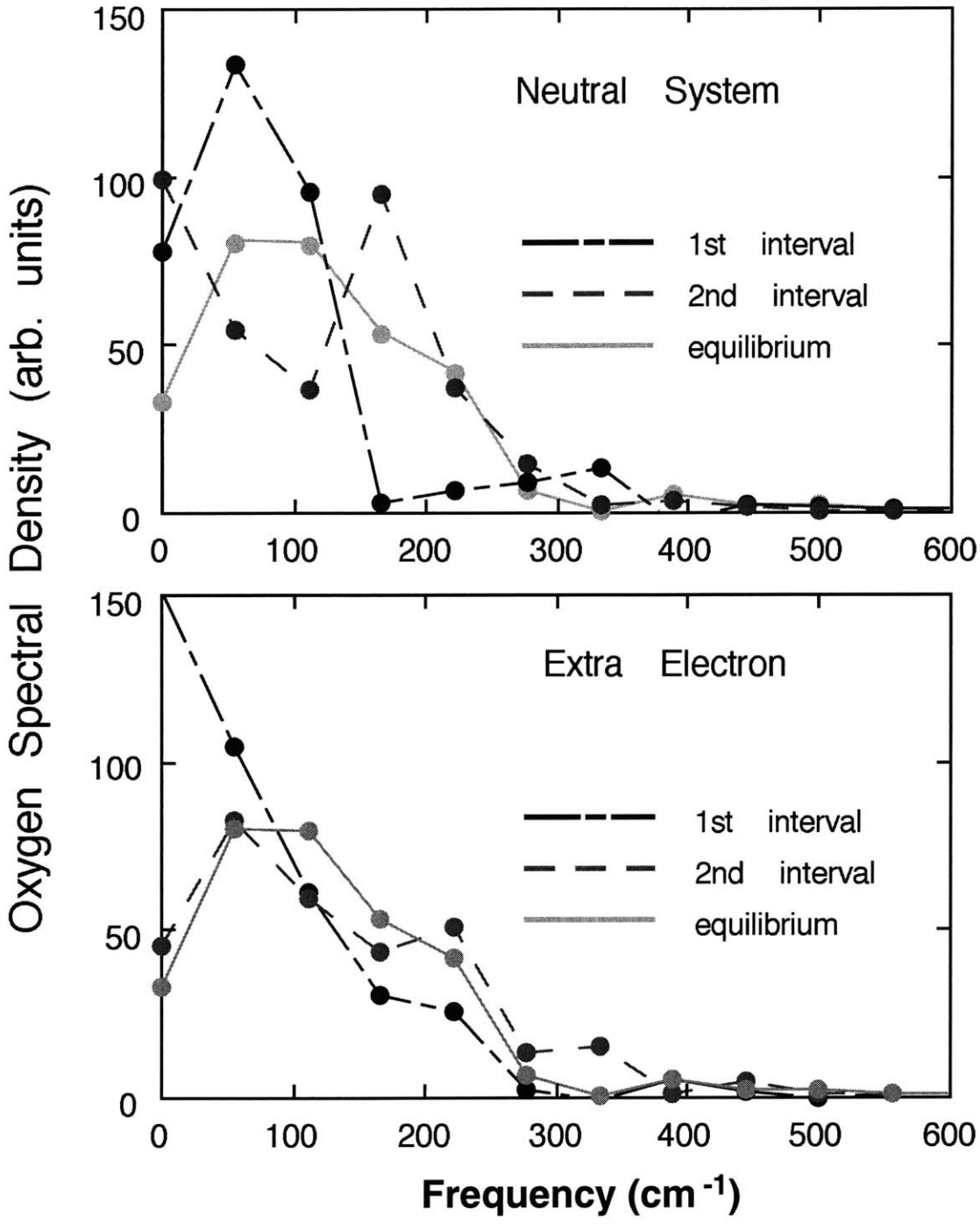


Figure 5-3: Spectral densities of oxygen velocity auto correlation functions for a neutral system (top panel) and for a system with an excess electron (bottom panel). In both cases, the doted (dashed) curves correspond to the 1st (2nd) time interval of 150 fsec relaxation from an initial Triangular Rings hexamer structure. The solid curve is the equilibrium spectral density of bulk water.

saturated by the excess electron charge distribution, lowering the energy barrier, and thus leading to the easier break-up of the original TR cavity.

To obtain a measure of the influence of the electron-dangling hydrogen atom interaction on the hydrogen atoms comprising the Kevan-like structure, we have calculated hydrogen velocity auto correlation functions. In Fig. 5-4, the spectral density after 1.4 psec originating from the hydrogen atoms located near the excess electron (solid curve) is compared with the corresponding spectral density of bulk water without an excess electron (doted curve). The calculated vibrational peaks at 1749cm$^{-1}$ and 3620cm$^{-1}$ for the neutral system are within 2% of experimental values [80]. The excess electron system shows peaks at 1708cm$^{-1}$, 3513cm$^{-1}$, and 3624cm$^{-1}$. The difference between neutral and excess electron systems can be attributed to the attractive interaction between the excess electron and neighboring hydrogens. Note, that the significant increase in weight of H-O-H bending modes around 1708cm$^{-1}$ is most likely caused by the active rotational motions of water molecules nearby the excess electron.

Thus the results of both oxygen and hydrogen spectral densities reveal that the dominant influence of the excess electron is in the orientational dynamics rather than the translational dynamics of the surrounding water molecules. Finally, although the purpose of this work is not to calculate the diffusion constants of bulk water and the electron, we can still get rough estimates from the 2 psec run. To determine these diffusion constants we calculated conventional mean square displacements as a function of time [70]. Our calculated water self diffusion constant of 2.6$\pm$0.3 $\times$ 10$^{-5}$cm$^2$/sec is within 10% of experiment [81] and the solvated electron diffusion constant is calculated to be 5.0$\pm$0.8 $\times$ 10$^{-5}$ cm$^2$/sec which is in agreement with the experimental value of 4.9$\pm$0.5 $\times$ 10$^{-5}$ cm$^2$/sec [82]. In Fig. 5-5 we plot the data and linear fit which we used to obtain the electron diffusion constant.

### 5.3.2 Electron Transport Mechanism.

Throughout the simulation described in 5.2.2, we again find that a Kevan-like geometry is stably maintained, on the average, with molecules exchanging at the surface

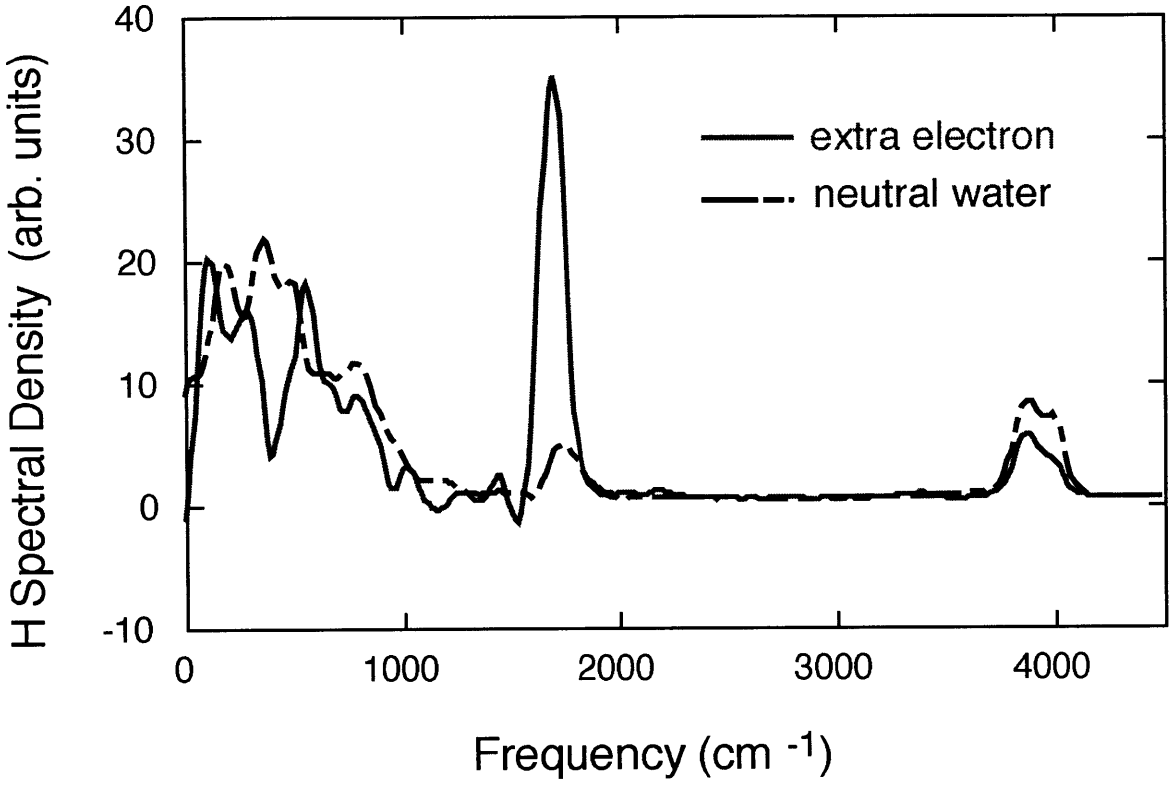


Figure 5-4: Spectral densities of hydrogen velocity auto correlation functions for water molecules comprising a Kevan-like structure surrounding an excess electron (solid) and for bulk equilibrated water (doted). The solid curve is calculated after 1.4 psec run. The frequency, which shows a dramatic increase in solid curve, corresponds to the H-O-H bending modes of water molecules.

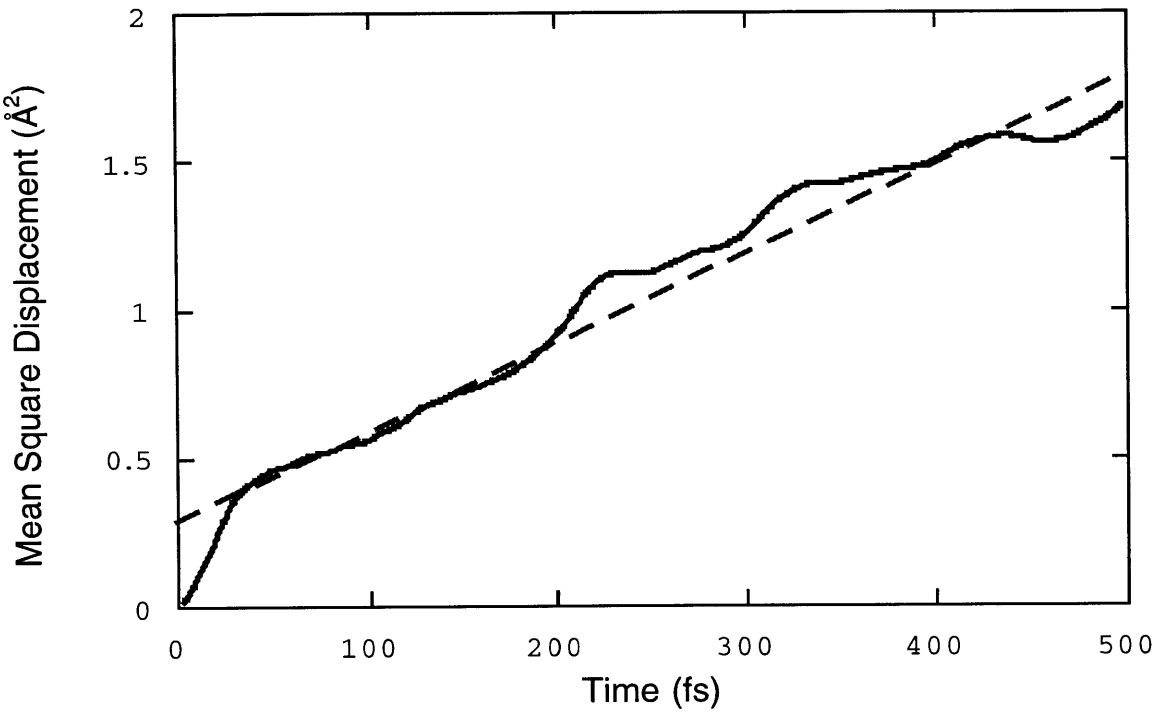


Figure 5-5: Mean square displacement of center of charge as a function of time for an excess electron in water. In order to ensure proper equilibrium of the excess electron, the mean square displacement is calculated using the final psec data of the 2 psec run described in the text. The configuration averaging was performed over 500 fsec for each time point plotted in the figure. The dashed line represents a linear fit of $\langle \Delta r^2 \rangle \sim 6Dt$ that provides a diffusion constant of $5.0 \times 10^{-5}$ cm$^2$/sec.

of the cavity. Ideally, one would like to replace the pseudo-molecules with hydrogen and oxygen atoms when they enter the first Kevan-like shell and vice versa when they exit the shell. However, this is unnecessary for our purposes since we wish to focus only on the detailed short-time evolution of the excess electron, in which a significant number of hydrogen and oxygen atoms still interact strongly with the electron.

In Fig. 5-6, we show the results of the *ab initio* simulations for snap-shots at (a) 20 fsec, (b) 40 fsec, and (c) 60 fsec after the 2 psec effective equilibration. The brighter water molecules represent the six water molecules replaced by atomic pseudopotentials. They are tagged in this fashion to help the reader visualize the evolution of the electron at 20 fsec and 40 fsec later. There are several important aspects of the electron transport that emerge from these results. For example, we note that the centers-of-mass of the water molecules do not move significantly during the 40 fsec time-interval spanned in the figure. Nevertheless, the electron has clearly moved to the right and a new Kevan-like structure can now be defined. This motion of the electron is driven by the *rotation* of the water molecules. Indeed, these results clearly demonstrate that it is the dangling hydrogen atoms that are driving the transport process of an electron in bulk water. As we proceed from Fig. 5-6(a) to 5-6(c), the dangling hydrogen atoms of water molecules labeled 1 and 2 are rotating away from the electron. Although it is not clear from the figure, these dangling hydrogen atoms are actually in the process of forming hydrogen bonds with other molecules. This tends to repel the electron from these hydrogen atoms. On the other hand, a hydrogen atom of water molecule 3 is in the process of rotating to break a hydrogen bond. The electron is then attracted to what eventually becomes a dangling hydrogen atom.

Thus the emerging picture of transport is perhaps what might best be described as a random opportunistic walk in which the electron is attracted to hydrogen atoms in the process of becoming dangling and repelled by dangling hydrogen atoms in the process of forming hydrogen bonds. This does not mean to imply that the electron is completely at the mercy of the molecular rotations. If this were the case, the electron would not form a coherent cavity-like structure. Instead, the transport of the electron involves a much more cooperative effect. Thermal fluctuations initiate

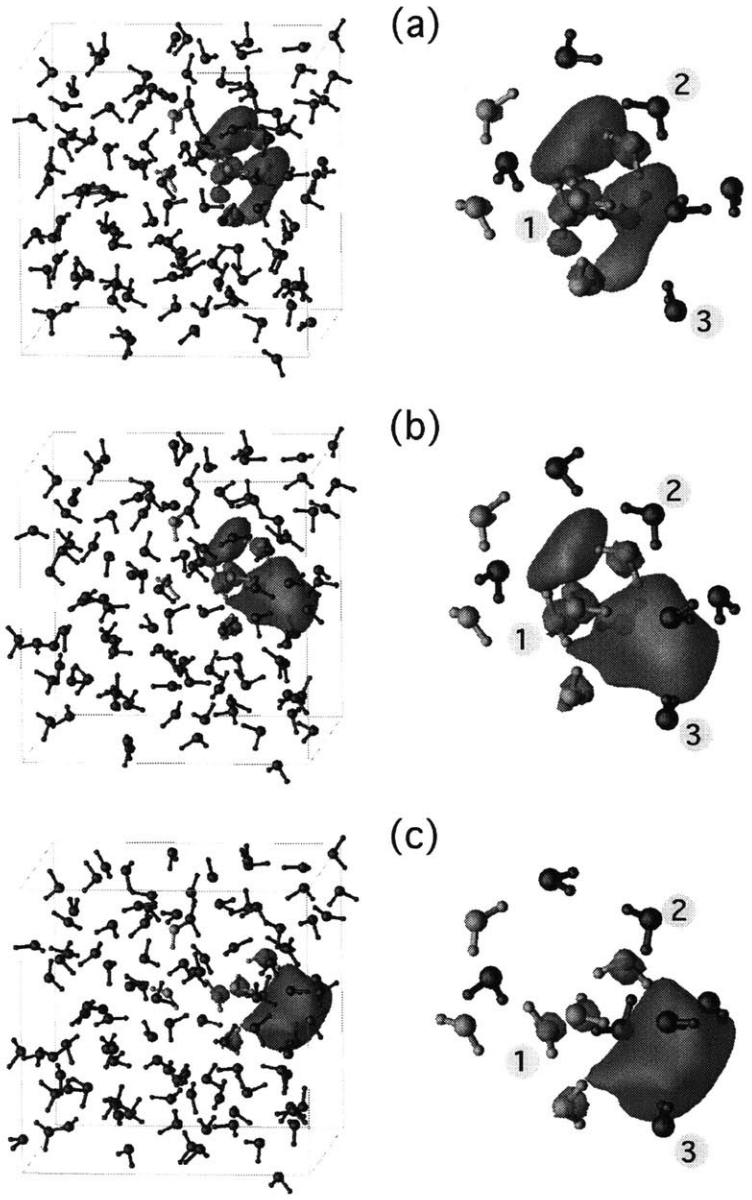


Figure 5-6: Room temperature *ab initio* dynamical simulation of 106 pseudo water molecules, 12 hydrogen atoms, 6 oxygen atoms, and an excess electron in a cubic super-cell at (a) 20 fsec, (b) 40 fsec, and (c) 60 fsec after a 2 psec effective equilibration. The excess electron charge distribution is shown as the isosurface and the six water molecules described by ionic pseudo-potentials are tagged to be brighter. Note how the electron moves to the right in a time-interval of 40 fsec

the weakening of a nearby hydrogen bond to which the electron is attracted, thereby attracting additional hydrogen atoms to the new location of the electron. Similarly, thermal fluctuations that strengthen a hydrogen bond repel the electron into a new location with a corresponding feedback effect.

Interestingly, if we go back to the first set of less accurate calculations, we can identify precisely the same type of transport mechanism. Moreover, although a comparison of Figs. 5-2(b) and 5-6(c) would seem to imply different diffusion times, these figures only represent a small portion of the diffusion motion for each set of simulations. A calculation of the approximate diffusion constants for each set reveals that they differ by less than 30%.

## 5.4 Conclusion

This new picture gives us a qualitative understanding of why the solvated electron diffusion constant is so much larger than that of solvated anions (e.g. $Br^-$). In the latter case, the diffusion process is clearly limited by the *center-of-mass* diffusion of the water molecules rather than their *rotational* dynamics. This picture also distinguishes the excess electron transport from that of protons and hydroxyl ions where fast diffusion is also possible. In the case of protons and hydroxyl ions the diffusion mechanism involves rotational rearrangements but the limiting steps are in ion-complex formation/dissociation and exchange [83]. Such formation/dissociation and exchange processes are not relevant for the electron transport mechanism identified in this work.

# Bibliography


[1] P. Hohenberg and W. Kohn, Phys. Rev. **136**, 864B (1964).

[2] W. Kohn and L.J. Sham, Phys. Rev. **140**,1133A (1965).

[3] E.P. Wigner, Trans. Faraday Soc. **34**, 678 (1938).

[4] L. Hedin and B. Lundqvist, J. Phys. C **4**, 2064 (1971).

[5] S.H. Vosko, L. Wilk, and M. Nusair, Can. J. Phys. **58**, 1200 (1980).

[6] J.P. Perdew and A. Zunger, Phys. Rev. B **23** 5048 (1981).

[7] J.P. Perdew, Phys. Rev. B **33**, 8822 (1986).

[8] A.D. Becke, Phys. Rev. A **30**, 3098 (1988).

[9] J. P. Perdew, J.A. Chevary, S.H. Vosko, K.A. Jackson, M.R. Pederson, D.J. Singh, and C. Fiolhais, Phys. Rev. B **46**, 6671 (1992).

[10] J.P. Perdew, K. Burke, and M. Ernzerhof, Phys. Rev. Lett. **77**, 3865 (1996).

[11] J.C. Phillips, Phys. Rev. **112**, 685 (1958).

[12] M.L. Cohen and V. Heine, Solid State Physics **24**, 37 (1970).

[13] M.T. Yin and M.L. Cohen, Phys. Rev. B **25**, 7403 (1982).

[14] Vasily V. Bulatov and Efthimios Kaxiras, Phys. Rev. Lett. **78**, 4221 (1997); P.A. Marrone, T.A. Arias, W.A. Peters, and J.W. Tester, J. Phys. Chem. A **102**, 7013 (1998)

[15] J. Harris and R.O. Jones, J. Phys. F **4**, 1170 (1974).

[16] O. Gunnarsson and B. I. Lundqvist, J. Phys. C **4**, 4174 (1976).

[17] D.C. Langreth and J.P. Perdew, Phys. Rev. B **15**, 2884 (1977).

[18] D.C. Langreth and J.P. Perdew, Phys. Rev. B. **21**, 5469 (1980); D.C. Langreth and M.J. Mehl, Phys. Rev. B **8** 1809 (1983); C.D. Hu and D.C. Langreth, Phys. Scr. **32**, 391 (1985).

[19] D.J. Chadi and M. L. Cohen, Phys. Rev. B **8**, 5747 (1973); J.D. Joannopoulos and M.L. Cohen, J. Phys. C **6**, 1572 (1973); H.J. Monkhorst and J.D. Pack, Phys. Rev. B **13**, 5188 (1976); R.A. Evarestov and V.P. Smirnov, Phys. Status Solidi **119**, 9 (1983).

[20] G.P. Francis and M.C. Payne, J. Phys: Condense. Matter **17**, 1643 (1990); G.M. Rignanese, Ph. Ghosez, J.C. Charlier, J.P. Michenaud, and X. Gonze, Phys. Rev. B **52**, 8160 (1995).

[21] E. Fermi, Nuovo Cimento **11**, 157 (1934).

[22] J.C. Phillips and L. Kleinman, Phys. Rev. **116**, 287 (1959).

[23] D.R. Hamann, M. Shlüter, and C. Chiang, Phys. Rev. Lett. **43**, 1494 (1979).

[24] G. Kerker, J. Phys. C **13**, L189 (1980).

[25] G.B. Bachelet and M. Cshlüter, Phys. Rev. B **25**, 2103 (1982); G.B. Bachelet, D.R. Hamann, and M. Schlüter, Phys. Rev. B **26**, 4199 (1982).

[26] L. Kleinman, Phys. Rev. **21**, 2630 (1980).

[27] A.M. Rappe, K.M. Rabe, E. Kaxiras, and J.D. Joannopoulos, Phys. Rev. B **41**, 1227 (1990).

[28] N. Troullier and J. L. Martins, Phys. Rev. B **43**, 1993 (1991).

[29] E. L. Shirley, D.C. Allan, R.M. Martin, and J.D. Joannopoulos, Phys. Rev. B **40**, 3652 (1989).

[30] Leonard Kleinman and D. M. Bylander, Phys. Rev. Lett. **48**, 1425 (1982).

[31] P.E. Blöchl, Phys. Rev. B **41**, 5414 (1990).

[32] M.Y. Chou, Phys. Rev. B **45**, 11465 (1992).

[33] P.P. Ewald, Ann. Phys.(Leipzig) **64**, 253 (1921).

[34] M.T. Yin and M.L. Cohen, Phys. Rev. B **26**, 5668 (1982).

[35] R. Car and M. Parrinello, Phys. Rev. Lett. **55**, 2471 (1985).

[36] M. C. Payne, M. P. Teter, D. C. Allan, T. A. Arias, and J. D. Joannopoulos, Rev. Mod. Phys. **64**, 1045 (1992).

[37] H. Hellmann, *Einfuhrung in die Quantumchemie* (Deuticke, Leipzig, 1937).

[38] R.P. Feynman, Phys. Rev. **56**, 340 (1939).

[39] *Theory of Chemisorption*, edited by J. R. Smith (Springer-Verlag, Berlin, 1980).

[40] R. Wolkow and Ph. Avouris, Phys. Rev. Lett. **60**, 1049 (1988); Ph. Avouris and R. Wolkow, Phys. Rev. B **39**, 5091 (1989).

[41] K. Takayanagi, Y. Tanishiro, M. Takahashi, and S. Takahashi, J. Vac. Sci. Technol. A **3**, 1502 (1985).

[42] K. D. Brommer, M. Needels, B. E. Larson, and J. D. Joannopoulos, Phys. Rev. Lett. **68**. 1355 (1992).

[43] I. Štich, M. C. Payne, R. D. King-Smith, J. S. Lin, and L. J. Clarke, Phys. Rev. Lett. **68**, 1351 (1992).

[44] K. D. Brommer, M. Galvan, A. Dal Pino Jr., and J. D. Joannopoulos, Surf. Sci. **314**, 57 (1994).

[45] K. D. Brommer, B. E. Larson, M. Needels, and J. D. Joannopoulos, Computers in Physics **7**, 350 (1993). and J. D. Joannopoulos, Phys. Rev. B **41**, 1227 (1990).

[46] C. G. Van de Walle, Phys. Rev. B **49**, 4579 (1994).

[47] E. Kaxiras and J. D. Joannopoulos, Phys. Rev. B **37**, 8842 (1988).

[48] D. C. Allan, J. D. Joannopoulos, and W. B. Pollard, Phys. Rev. B **25**, 1065 (1982).

[49] R. Wolkow (private communication).

[50] H. Haberland, Ed. Clusters of Atoms and Molecules (Springer-Verlag, Berlin, 1994); M. Armbruster, H. Haberland, H.-G. Schindler, Phys. Rev. Lett. **47**, 323 (1981); D. Emin, Phys. Today, **35**, 34 (1982); P.J. Rossky and J. Schnitker, J. Phys. Chem. **92**, 4277 (1988); R.N. Barnett, U. Landman, D. Scharf, J. Jortner, Acc. Chem. Res. **22**, 350 (1989); Z. Deng, G.J. Martyna, M.L. Klein, Phys. Rev. Lett. **71**, 267 (1993); D. Chandler and K. Leung, Ann. Rev. Phys. Chem. **45**, 557 (1994).

[51] L. Kevan, Acc. Chem. Res. **14**, 138 (1981).

[52] E.J. Hart and J.W. Boag, J. Am. Chem. Soc. **84**, 4090 (1962); J.P. Keene, Nature, **197**, 147 (1963).

[53] R.N. Barnett, U. Landman, C.L. Cleveland, J. Jortner, Phys. Rev. Lett. **59**, 811 (1987); J. Chem. Phys. **88**, 4429 (1988).

[54] J.V. Coe, G.H. Lee, J.G. Eaton, S.T. Arnold, H.W. Sarkas, K.H. Bowen, C. Ludewigt, H. Haberland, and D.R. Worsnop, J. Chem. Phys. **92**, 3980 (1990); G.H. Lee, S.T. Arnold, J.G. Eaton, H.W. Sarkas, K.H. Bowen, C. Ludewigt, H. Haberland, Z. Phys. D. **20**, 9 (1991).

[55] C. Desfrancois, A. Lisfi, J.P. Schermann, Z. Phys. D. **24**, 297 (1992); C. Desfrancois, N. Khelifa, A. Lisfi, J.P. Schermann, J.G. Eaton, K.H. Bowen, J. Chem. Phys. **95**, 7760 (1991); F. Misaizu, T. Kondow, K. Kuchitsu, Chem. Phys. Lett.

**178**, 369 (1991); M. Knapp, O. Echt, D. Kreisle, E. Recknagel, J. Phys. Chem. **91**, 2601 (1987).

[56] T. Clark and G. Illing, J. Am. Chem. Soc. **109**, 1013 (1987); B.K. Rao and N.R. Kestner, J. Chem. Phys. **80**, 1587 (1984); N.R. Kestner and J. Jortner, J. Phys. Chem. **88**, 3818 (1984).

[57] H. Tachikawa, A. Lund, M. Ogasawara, Can. J. Chem. **71**, 118 (1993).

[58] A. T. Pudzianowski, J. Chem. Phys. **102**, 8029 (1995).

[59] W.J. Hehre, L. Radom, P. von R. Schleyer, J.A. Pople, *Ab initio* molecular orbital theory (Wiley-Interscience, New York, 1986).

[60] J. Schnitker, K. Motakabbir, P.J. Rossky, R. Friesner, Phys. Rev. Lett. **60**, 456(1988).

[61] B.J. Mhin, H.S. Kim, H.S. Kim, C.W. Yoon, K.S. Kim, Chem. Phys. Lett. **176**, 41 (1991); K.A. Franken, M. Jalaie, C.E. Dykstra, *ibid.* **198**, 59 (1992); C.J. Tsai and K.D. Jordan, *ibid.* **131**, 451 (1993); B.J. Mhin, J. Kim, S. Lee, J.Y. Lee, K.S. Kim, J. Chem. Phys. **100**, 4484 (1994).

[62] K.S. Kim and E. Clementi, J. Am. Chem. Soc. **107**, 5504 (1985); K.S. Kim, H.L. Nguyen, P.K. Swaminathan, E. Clementi, J. Phys. Chem. **89**, 2870 (1985).

[63] H. Nar, A. Messerschmidt, R. Huber, M. van de Kamp, G.W. Canters, J. Mol. Biol. **218**, 427 (1991).

[64] *Solvated Electron*, edited by R. F. Gould (American Chemical Society, Washington, 1965).

[65] *Electron-Solvent and Anion-Solvent Interactions*, edited by Kevan and Webster (Elsevier Scientific, New York, 1976).

[66] *Radiation Chemistry: Principles and Applications*, edited by Farhataziz and M. A. Rodgers (VCH, New York 1987).

[67] F. H. Long, H. Lu, and K. B. Eisenthal, Phys. Rev. Lett. **64**, 1469 (1990).

[68] P. J. Rossky and J. Schnitker, J. Phys. Chem. **92**, 4277 (1988); F. J. Webster, J. Schnitker, M. S. Friedrichs, R. A. Friesner, and P. J. Rossky, Phys. Rev. Lett. **66**, 3172 (1991); T. H. Murphrey and P. J. Rossky, J. Chem. Phys. **99**, 515 (1993).

[69] E. Neria, A. Nitzan, R. N. Barnett, and U. Landman, Phys. Rev. Lett. **67**, 1011 (1991).

[70] G. S. Del Buono, P. Rossky, and T. H. Murphrey, J. Phys. Chem. **96**, 7761 (1992).

[71] R. W. Impey, P. A. Madden and I. R. McDonald, J. Phys. Chem. **87**, 5071 (1983).

[72] W. F. Schmidt in Ref. [65].

[73] Jurgen Schnitker and P. J. Rossky, J. Phys. Chem. **93**, 6965 (1983); G. S. Del Buono, P. J. Rossky and T. H. Murphy, J. Phys. Chem. **96**, 7761 (1992).

[74] R. N. Barnett, U. Landman, and A. Nitzan, J. Chem. Phys. **93**, 8187 (1990); H. Kaukonen, R. N. Barnett, and U. Landman, J. Chem. Phys. **97**, 1365 (1992)

[75] K. S. Kim, I. Park, S. Lee, K. Cho, J. Lee, J. Kim, and J. D. Joannopoulos, Phys. Rev. Lett. **76**, 956 (1996).

[76] S. Lee, J. Kim, S. Lee, and K. S. Kim, Phys. Rev. Lett. **79**, 2048 (1997).

[77] C. G. Bailey, J. Kim, and M. A. Johnson, J. Phys. Chem. **100**, 16782 (1996).

[78] G. C. Lie and E. Clementi, Phys. Rev. A **33**, 2679 (1986).

[79] T.A. Arias, M.C. Payne, and J.D. Joannopoulos, Phys. Rev. Lett. **69**, 1077 (1992).

[80] D. Eisenberg and W. Kauzmann, *The Structure and Properties of Water* (Oxford University, New York, 1969).

[81] K. Krynicki, C. D. Green, and D. W. Sawyer, Faraday Disscuss. Chem. Soc. **66**, 199 (1978).

[82] K. H. Schmidt and W. L. Buck, Science **151**, 70 (1966); G. C. Barker, P. Fowles, D. C. Sammon, and B. Stringer, Trans. Faraday Soc. **66**, 1498 (1970).

[83] K. Kreuer, Chem. Mater. **8**, 610 (1996); R. G. Schmidt and J. Brickmann., Ber. Bunsenges. Phys. Chem. **101**, 1816 (1997).